

RESEARCH ARTICLE

Genetic deletion of *hspa8* leads to selective tissue malformations in zebrafish embryonic development

Caixia Wang^{1,2}, Xin Zhang^{1,2}, Xinyu Wang^{1,2}, Yanpeng Zhai^{1,2}, Mengjiao Li^{1,2}, Jun Pan^{1,2}, Yan Bai¹, Xiaozhi Rong^{1,2,*} and Jianfeng Zhou^{1,2,*}

ABSTRACT

The heat shock cognate 71 kDa protein HSPA8 (also known as HSC70), a constitutively expressed cognate member of the heat shock protein 70 family, plays an essential role in protein quality control and cell homeostasis maintenance. HSPA8 has been implicated in many diseases, including cancers and neurodegenerative diseases. Owing to massive cell death after knockdown of *HSPA8* and nonviable *Hspa8* knockout mice, the physiological role of HSPA8 in vertebrates and its underlying mechanisms of action have not yet been elucidated. To address this issue, we used CRISPR/Cas9 technology and genetically deleted *hspa8* in zebrafish embryos. Genetic deletion of *hspa8* resulted in malformations of the pharyngeal arches, pectoral fins, head and eyes at the later stages. We next focused on pharyngeal arch deficiency and found that pharyngeal arches in *hspa8* mutant embryos exhibited induction of endoplasmic reticulum stress and activation of the unfolded protein response via the Perk/p-eIF2 α /Atf4 signaling cascade. Inhibition of Perk/p-eIF2 α /Atf4 signaling rescued the developmental deficiency of pharyngeal arches caused by depletion of *Hspa8*. Taken together, our results provide novel insights into the tissue-specific roles of *Hspa8* in the regulation of vertebrate embryonic development.

KEY WORDS: *Hspa8*, Hsc70, p53, Pharyngeal arch cartilages, Zebrafish, CRISPR/Cas9, Endoplasmic reticulum stress, Unfolded protein response, EIF2 α , ATF4

INTRODUCTION

Cranial neural crest cells (NCCs) are transient cell types that originate in the dorsal region of neural folds during vertebrate embryogenesis. Following epithelial to mesenchymal transition, NCCs migrate to the craniofacial region. Next, the post-migratory NCCs differentiate into numerous cell and tissue types and form nearly all craniofacial structures, including the facial skeleton and the majority of facial connective tissues (Minoux and Rijli, 2010).

The heat shock cognate 71 kDa protein HSPA8, also named HSC70, is a constitutively expressed cognate member of the heat

shock protein 70 family. It facilitates the folding of proteins and maintains their normal structures and functions (Liu et al., 2012). HSPA8 is extremely abundant in cells and represents up to 1% of the total cellular protein content (Bonam et al., 2019; Stricher et al., 2013). As a chaperone protein, HSPA8 interacts with numerous molecules and is involved in diverse biological functions in cells, such as protein folding, neo-protein synthesis and protein translocation, as well as degradation, to maintain cell homeostasis (Liu et al., 2012; Stricher et al., 2013). Dysregulation of HSPA8 has been previously shown to be associated with various clinical diseases, including neurodegenerative diseases, cardiac diseases, stroke, metabolic diseases, cancer, asthma and aging (Bonam et al., 2019; Liu et al., 2012; Stricher et al., 2013). However, the mechanism underlying these diseases remains largely unknown. HSPA8 is regarded as an essential protein for cell survival because *HSPA8* knockdown results in massive cell death in a variety of cell lines (Florin et al., 2004; Rohde et al., 2005), suggesting that *Hspa8*-knockout mice cannot be generated, which limits our understanding of the physiological role of HSPA8 (Bonam et al., 2019; Daugaard et al., 2007). Given that HSPA8 is evolutionarily conserved and plays an essential role in cell survival, an alternative experimental model organism is needed to explore the physiological role of HSPA8 in vertebrates.

Zebrafish embryos are suitable for observing phenotypic changes in real time owing to their rapid *ex utero* development and transparency. Therefore, zebrafish embryos are an excellent model organism for clarifying the molecular and cellular basis underlying the physiological role of essential genes. Because *HSPA8* knockdown typically results in cell death in mammals, investigations of the role of HSPA8 and its underlying mechanisms have been challenging. To overcome this challenge, this study employed CRISPR/Cas9 to obtain an *hspa8*-knockout zebrafish model. This approach allows for exploring the physiological effects of *hspa8*-knockout during embryogenesis as well as investigation of the mechanisms involved in these effects. In this study, we showed that genetic deletion of *hspa8* leads to tissue-selective developmental deficiency. We next paid attention to the severe loss of pharyngeal arch (PA) cartilage in the *Hspa8*-depleted embryos at the NCC post-migration stage and found that Perk/p-eIF2 α /Atf4 signaling, a branch of the unfolded protein response (UPR) signaling cascade, is activated in PA cartilage in *hspa8* mutant embryos. Our findings illustrate how disruption of *Hspa8* leads to PA cartilage malformations and suggest that elevated Perk/p-eIF2 α /Atf4 signaling likely mediates the *Hspa8* deficiency-induced pathologies.


RESULTS

Genetic deletion of *hspa8* impairs PA cartilage formation

The zebrafish genome contains two *hspa8* genes, *hspa8* and *hspa8b* (Fig. S1A,B). We first performed RT-PCR analysis to detect

¹Key Laboratory of Marine Drugs (Ocean University of China), Chinese Ministry of Education, and School of Medicine and Pharmacy, Ocean University of China, 5 Yushan Road, Qingdao 266003, China. ²Laboratory for Marine Drugs and Bioproducts, Pilot National Laboratory for Marine Science and Technology (Qingdao), Qingdao 266003, China.

*Authors for correspondence (jfzhou@ouc.edu.cn; rongxiaozhi@ouc.edu.cn)

 C.W., 0000-0002-5790-7469; X.Z., 0000-0001-6631-6145; Y.Z., 0000-0002-4505-7807; J.P., 0000-0002-9822-7689; Y.B., 0000-0002-4982-7549; X.R., 0000-0002-8252-6289; J.Z., 0000-0001-5702-6664

temporal expression patterns of *hspa8* and *hspa8b* with specific primers (Fig. S1A). As shown in Fig. S2A, *hspa8* was maternally deposited and expressed at a relatively stable level during early developmental stages, whereas *hspa8b* was not detectable. In agreement with the RT-PCR data, analysis of data from a previous RNA-seq analysis showed that *hspa8* mRNA was abundant, whereas *hspa8b* mRNA levels were extremely low throughout embryogenesis [*hspa8*: 286 to 809 fragments per kilobase of exon per million mapped fragments (FPKM) versus *hspa8b*: 0 to 2 FPKM] (White et al., 2017; <https://www.ebi.ac.uk/gxa/experiments/E-ERAD-475/>). We next examined the Hspa8 protein at different developmental stages with an antibody against amino acids (aa) 580–601 at the C-terminus of human HSPA8 because the amino acid identity between HSPA8, Hspa8 and Hspa8b is high (Fig. S1B). Both GFP-tagged Hspa8 and Hspa8b was detected by this antibody, suggesting that this antibody recognizes endogenous Hspa8 and Hspa8b in zebrafish embryos (Fig. S2B). Western blot analysis showed that the Hspa8 protein was abundantly deposited and expressed throughout embryogenesis (Fig. S2C). Given that *hspa8b* mRNA was not detectable, the protein we detected was most likely Hspa8. Then, we explored the role of *hspa8* in embryonic development solely. Whole-mount *in situ* hybridization (WISH) analysis with an *hspa8* specific anti-sense probe revealed that *hspa8* transcripts were maternally deposited and ubiquitously expressed at all stages prior to 24 hours post fertilization (hpf). Furthermore, *hspa8* transcripts were enriched in PAs, eyes, pectoral fins, and posterior tectum at later stages, including at 24, 48, 72 and 96 hpf (Fig. S2D).

To determine the physiological role of Hspa8 during embryogenesis, we generated three *hspa8* knockout zebrafish lines with two different target sites on exon 2 and exon 3 (Fig. S3A). The three lines were all null mutants with frame-shift mutations that led to premature stop codons and caused the production of truncated HSPA8 with 141 aa, 139 aa and 12 aa (Fig. 1A; Fig. S3B). The *hspa8* zygotic mutant embryos died ~10–12 days post fertilization. We could not obtain adult homozygous mutant fish to generate maternal-zygotic mutant embryos to eliminate maternally derived mRNA or protein for phenotypic analysis. Therefore, the phenotype of zygotic mutant embryos was analyzed.

Semi-quantitative RT-PCR analysis showed that *hspa8* transcripts were greatly decreased in *hspa8* mutants both at 72 and 96 hpf, which might be caused by nonsense-mediated mRNA decay (Fig. 1B). Therefore, we conclude that the alleles are null alleles. However, western blot analysis showed that Hspa8 protein levels were severely reduced but not completely lost in *hspa8* mutants both at 72 and 96 hpf (Fig. 1C). Recent studies reported that premature termination codons in zebrafish mutants can activate a compensation mechanism by upregulating the expression of other family members (El-Brolosy et al., 2019; Ma et al., 2019). Indeed, the mRNA levels of *hspa8b* were increased in *hspa8* mutant embryos at 72 and 96 hpf (Fig. S4A). Therefore, the protein we detected in *hspa8* mutant embryos likely contains Hspa8b as well as the possibly remaining Hspa8.

We further examined the phenotypes of *hspa8* mutant embryos during early embryonic development. No overt morphological changes were observed in the mutant embryos at 24 hpf (Fig. 1D). At 48, 72 and 96 hpf, the mutant embryos showed gradually reduced PAs, with a concomitant decrease in the pectoral fins, head and eyes when compared to that in their wild-type (WT) siblings (Fig. 1D,E). The PA reduction observed in mutant embryos was further confirmed by immunostaining with an anti-Col2 antibody (detecting collagen type II) in *Tg(fli1:EGFP)* transgenic

embryos, which express GFP in the post-migratory NCCs in the PAs and blood vessels (Fig. 1F,G) (Lawson and Weinstein, 2002).

Next, we carried out Alcian Blue staining to detect cartilage defects in *hspa8* mutant embryos at 72 and 96 hpf. As shown in Fig. 1H,I, *hspa8* mutant embryos showed almost complete loss of cartilage in all PAs at these stages. However, depletion of Hspa8 had no apparent effects on the formation of neurocranial cartilages, including the ethmoid plate, parachordal cartilages and trabeculae. Taken together, these results suggest that genetic deletion of *hspa8* abrogates the formation of PA cartilages.

Genetic deletion of *hspa8* affects PA cartilage development

The absence of PA cartilage in *hspa8* mutant embryos strongly suggested that the craniofacial NCCs were affected after *hspa8* was deleted. To determine which steps of cartilage formation were affected, we performed WISH assessment with several NCC markers labeling the induction and/or specification, migration and differentiation of NCCs in WT sibling and *hspa8* mutant embryos at different stages. The expression of the early neural crest induction and/or specification markers *foxd3* and *sox9a* appeared no difference between the WT and *hspa8* mutant embryos at 12 hpf, indicating that genetic deletion of *hspa8* had little to no effect on neural crest induction (Fig. 2A) (Hochgreb-Hagele and Bronner, 2013; Yan et al., 2002).

Next, we assessed whether NCC migration was affected. The expression of three indicative markers, *crestin* (the pan-neural crest marker expressed first in pre-migratory and then in actively migrating NCCs), *dlx2a* (expressed in the migrating cranial NCCs that contribute to PAs) and *sox10* (a transcription factor involved in NCC migration and differentiation that also marks migrating NCCs in stripes on either side of the neural tube), were examined by WISH analysis (Dutton et al., 2001; Elsen et al., 2008; Li et al., 2018; Sen et al., 2018; Sperber et al., 2008). At 24 hpf, the expression of *crestin* did not exhibit a significant difference between WT sibling and *hspa8* mutant embryos (Fig. 2B). The *dlx2a*-expressing NCCs migrated into the PAs in both WT sibling and *hspa8* mutant embryos at 18, 24, 30 and 36 hpf (Fig. 2C), whereas *dlx2a* expression was slightly decreased in *hspa8* mutants at 48 hpf (Fig. 2C). The NCCs from WT sibling and *hspa8* mutant embryos also showed little difference in *sox10* expression at 16, 18 and 24 hpf (Fig. 2D). However, the expression of *sox10* was reduced in *hspa8* mutants at 48 hpf (Fig. 2D). Previous studies have suggested that Sox9a plays an important role in both early neural crest specification and chondrocyte differentiation (Yan et al., 2002, 2005). Compared with that in WT sibling embryos, the expression of *sox9a* in the PAs of *hspa8* mutant embryos was significantly decreased at 50, 60, and 72 hpf (Fig. 2E). Taken together, these results suggest that Hspa8 is critical for PA maturation during embryonic development.

Depletion of Hspa8 suppresses cell proliferation and has little effect on cell apoptosis in the pharyngeal arch region

The reduction of PAs in *hspa8* mutant embryos suggested that Hspa8 depletion likely plays a role in proliferation and/or apoptosis of PA cells. Hence, we used an anti-phospho-histone H3 (pH3) antibody to immunostain *hspa8* mutant embryos with a *Tg(fli1:EGFP)* transgenic background at 48 hpf to investigate cell proliferation in the PA regions. The number of pH3-positive cells in the PAs of mutants was considerably lower than that in WT siblings (Fig. 3A,B; Fig. S5A). These results suggest that Hspa8 depletion inhibits cell proliferation in PAs, leading to a reduction in the area of the PA regions.

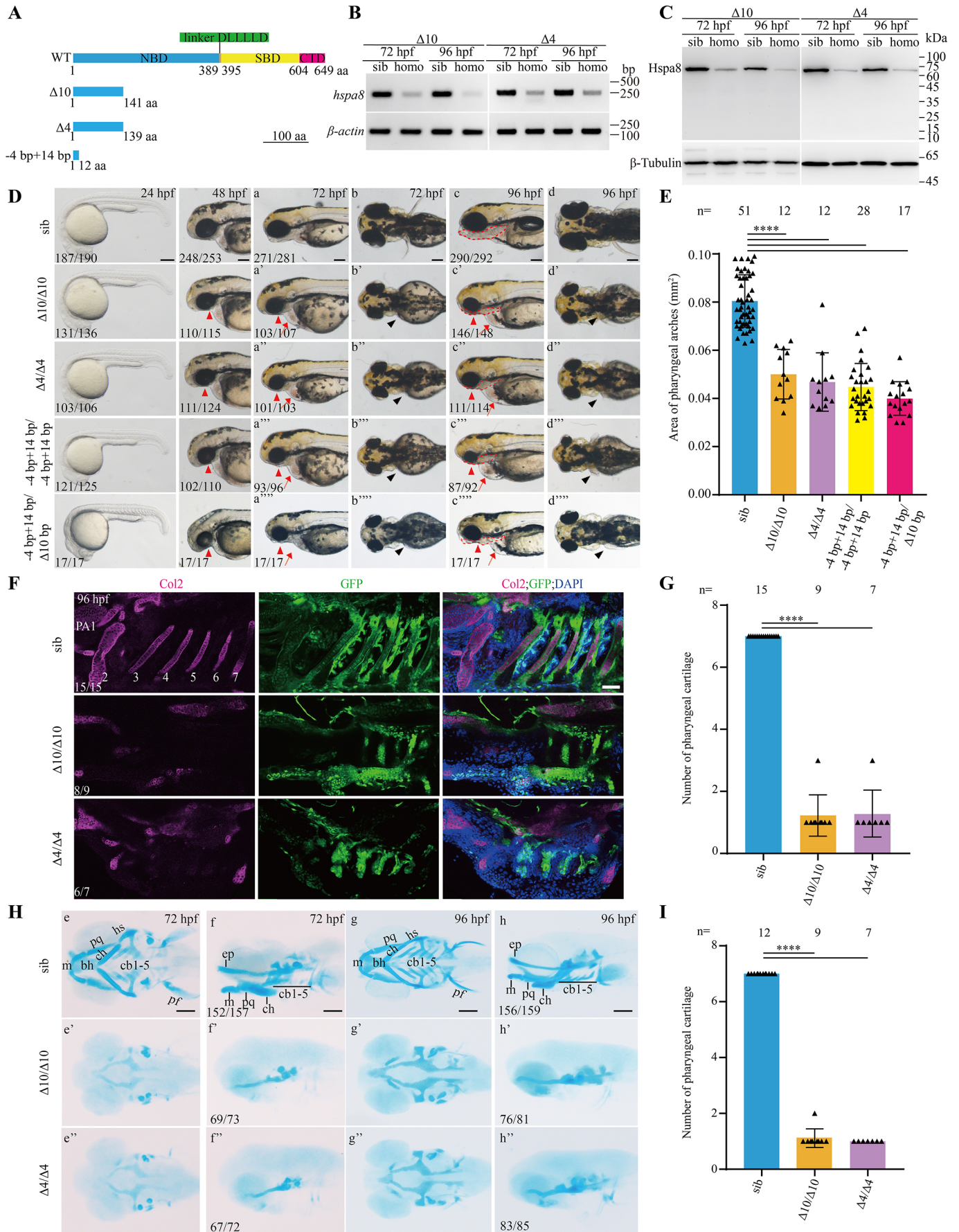


Fig. 1. See next page for legend.

Fig. 1. Genetic deletion of *hspa8* impairs the formation of pharyngeal arch cartilages. (A) Schematic diagram of Hspa8 protein domains and the *hspa8* mutant alleles ($\Delta 10$, $\Delta 4$ and -4 bp +14 bp) with predicted premature stop codons. NBD, nucleotide-binding domain; SBD, substrate-binding domain; CTD, C-terminal domain. (B) The mRNA levels of *hspa8* in siblings (sib) and homozygous *hspa8* mutants as indicated by semi-quantitative RT-PCR analysis. β -actin was used as an internal control. Similar results were obtained from three experiments. (C) Hspa8 protein levels in siblings and *hspa8* mutants. Tubulin was used as a loading control. Similar results were obtained from three experiments. (D) Representative images of WT siblings and *hspa8* mutants. The *hspa8* mutants exhibited microphthalmia (red arrowheads), edema of the pericardial cavity (red arrows), craniofacial jaw malformations, microcephaly, and reduction of pectoral fins (black arrowheads). The dashed lines mark the pharyngeal regions. Panels a–a' and c–c' represent lateral views, whereas panels b–b' and d–d' represent top views. Scale bars: 200 μ m. (E) Quantitative results of the area of pharyngeal regions of siblings and *hspa8* mutants at 96 hpf shown in D, c–c'. (F) Representative confocal images of WT sibling and *hspa8* mutant embryos at 96 hpf with a *Tg(fli1:EGFP)* transgenic background which were immunostained with an anti-Col2 antibody. Scale bar: 50 μ m. PA, pharyngeal arch. (G) Quantitative results of the number of pharyngeal arches shown in F. (H) Representative images of WT sibling and *hspa8* mutant head cartilage and pharyngeal arch cartilage stained with Alcian Blue. Scale bar: 200 μ m. Panels e–e' and g–g' represent ventral views, whereas panels f–f' and h–h' represent lateral views. m, Meckel's cartilage; hs, hyosymplectic; bh, basihyal; ch, ceratohyal; pq, palatoquadrate; cb, ceratobranchial; pf, pectoral fin; ep, ethmoid plate. (I) Quantitative results of the number of pharyngeal cartilages shown in H. The proportion of embryos with the indicated phenotypes is shown in the bottom left corner of each panel for D, F and H. Values are represented as means \pm s.d. **** $P < 0.0001$ (unpaired two-tailed *t*-test).

Next, we examined apoptosis in PA cells using two different approaches. Following immunostaining with an anti-active-caspase-3 antibody, we did not observe apoptotic cells in the PA region of *hspa8* mutant embryos with a *Tg(fli1:EGFP)* transgenic background at 48 hpf (Fig. 3C). In contrast, apoptotic cells were increased in the eyes (Fig. S5B). Similarly, with Acridine Orange (AO) staining, no apoptotic cells in the PA region were detected in *hspa8* mutant embryos at 48 hpf, although an increase in apoptotic cells was observed in the eyes (Fig. 3D). Therefore, it is likely that Hspa8 depletion does not affect the survival of cells in PAs. Collectively, these results indicated that cell- or tissue-specific responses occur after depletion of Hspa8 and that Hspa8 is critical to maintaining cell proliferation in PA development.

Depletion of Hspa8 upregulates p53 signaling

Mutations of housekeeping genes frequently activate the p53 tumor suppressor protein (Calo et al., 2018; Danilova et al., 2010). In the present study, depletion of Hspa8 also dramatically increased p53 protein expression levels (Fig. 4A). Next, we investigated whether *hspa8* knockout in zebrafish elevates the transcriptional level of p53 (also known as *tp53*). The p53 transcriptional level was increased in *hspa8*-deleted zebrafish embryos at 96 hpf, as indicated by quantitative real-time RT-PCR (qRT-PCR) analysis (Fig. 4B). To further confirm the activation of p53 protein after Hspa8 depletion, we examined the expression of p53 target genes, including *ccng1* (*cyclin G1*), $\Delta 113p53$ (encoding an N-terminally truncated p53 isoform), *cdkn1a* (*p21^{cip1/waf1}*) and *mdm2*, in zebrafish embryos at 96 hpf using qRT-PCR. Hspa8 depletion in zebrafish embryos increased the expression of *ccng1*, $\Delta 113p53$ and *cdkn1a*, whereas the expression of *mdm2*, a negative regulator of p53, was not altered (Fig. 4C). Taken together, these results suggest that Hspa8 depletion enhances the p53 signaling pathway *in vivo*.

Aberrant p53 activation during mice development has been shown to trigger cell cycle arrest or apoptosis, and therefore to result in diverse phenotypes, including craniofacial defects (Van Nostrand et al., 2014). In zebrafish, published WISH data suggest that p53 is expressed in various tissues, including PAs and pectoral fins of zebrafish embryos at 36, 48 and 84 hpf (Anderson et al., 2009; Hu et al., 2015; Yamaguchi et al., 2008). As mentioned above, *hspa8* mRNA signals were also enriched in these regions at 48, 72 and 96 hpf. To better understand the relationship between PA deficiency and p53 activation in *hspa8* mutant embryos, we therefore examined the time windows of p53 induction in PAs in *hspa8* mutant embryos from 30 to 48 hpf (Fig. 4D). We observed that the p53 expression level in PAs was robustly induced in *hspa8* mutant embryos from 42 to 48 hpf within manually dissected PA regions, as accessed by qRT-PCR (Fig. 4D). Consistent with this, the expression level of p53 in PAs was also markedly increased in *hspa8* mutant embryos from 42 to 48 hpf, as indicated by WISH (Fig. 4E). A similar effect was observed in the transcriptional levels of p53 target genes *ccng1* and $\Delta 113p53$, as indicated by qRT-PCR (Fig. 4F). Because the PA area in *hspa8* mutant embryos at late stages exhibited a reduction in proliferation and lack of apoptotic cells, we examined the expression levels of two distinct groups of p53 target genes – cell cycle arrest genes *cdkn1a* and *cdkn1bb* (*p27^{kip1}*) and proapoptotic genes *baxa*, *pmaip1* (*noxa*), *bida* and *bbc3* (*puma*) – in the PA region of WT sibling and *hspa8* mutant embryos at 48 hpf. Depletion of Hspa8 increased the transcriptional levels of *cdkn1a* and *cdkn1bb* (Fig. 4G). In contrast, the expression levels of *bida*, *baxa* and *pmaip1* were not increased, but the expression level of *bbc3* was (Fig. 4H). Taken together, these results further suggested that depletion of Hspa8 enhances the p53 signaling pathway in PAs *in vivo*.

Inactivation of p53 does not rescue PA deficiency caused by *hspa8* deletion

To confirm that depletion of Hspa8 induces p53 signaling activation, we manually dissected the anterior structures from sibling and *hspa8* mutant embryos at 96 hpf and compared the p53 protein levels. The p53 protein levels increased dramatically in homozygous embryos but not in WT or heterozygous embryos (Fig. 5A).

Given that depletion of Hspa8 leads to decreased cell proliferation in the PA area as well as activation of p53 signaling, we hypothesized that p53 activation might represent a key regulator of the PA area reduction caused by *hspa8* deletion. To investigate this hypothesis, we examined the phenotypes of *hspa8* mutants with a *p53^{M214K/M214K}* genetic background and investigated whether genetic ablation of p53 signaling could rescue the *hspa8* mutant phenotype. The *p53^{M214K}* mutation has been shown to affect the DNA-binding domain of p53 and diminish its transcriptional activation activity (Berghmans et al., 2005). We observed that, in *hspa8* mutants, p53 inactivation (*p53^{M214K/M214K}*) exhibited notable rescuing effects on morphological defects in eyes and pectoral fins but not on PA deficiency at 72 or 96 hpf (Fig. 5B,C). Likewise, p53 inactivation did not exhibit rescuing effects on PA deficiency in *hspa8* mutant embryos with a *Tg(fli1:EGFP)* transgenic background (Fig. 5D). Consistent with this, the expression of the NCC marker gene *sox9a* was not restored in *hspa8* mutant embryos with a *p53^{M214K/M214K}* genetic background at 50, 60, 72 and 96 hpf (Fig. 5E). To better understand the effect of p53 genetic inactivation on *hspa8* mutants, we next performed Alcian Blue staining to examine cartilage development in *hspa8* mutants with a *p53^{M214K/M214K}* genetic background. As shown in Fig. 5F,G, p53 inactivation did not

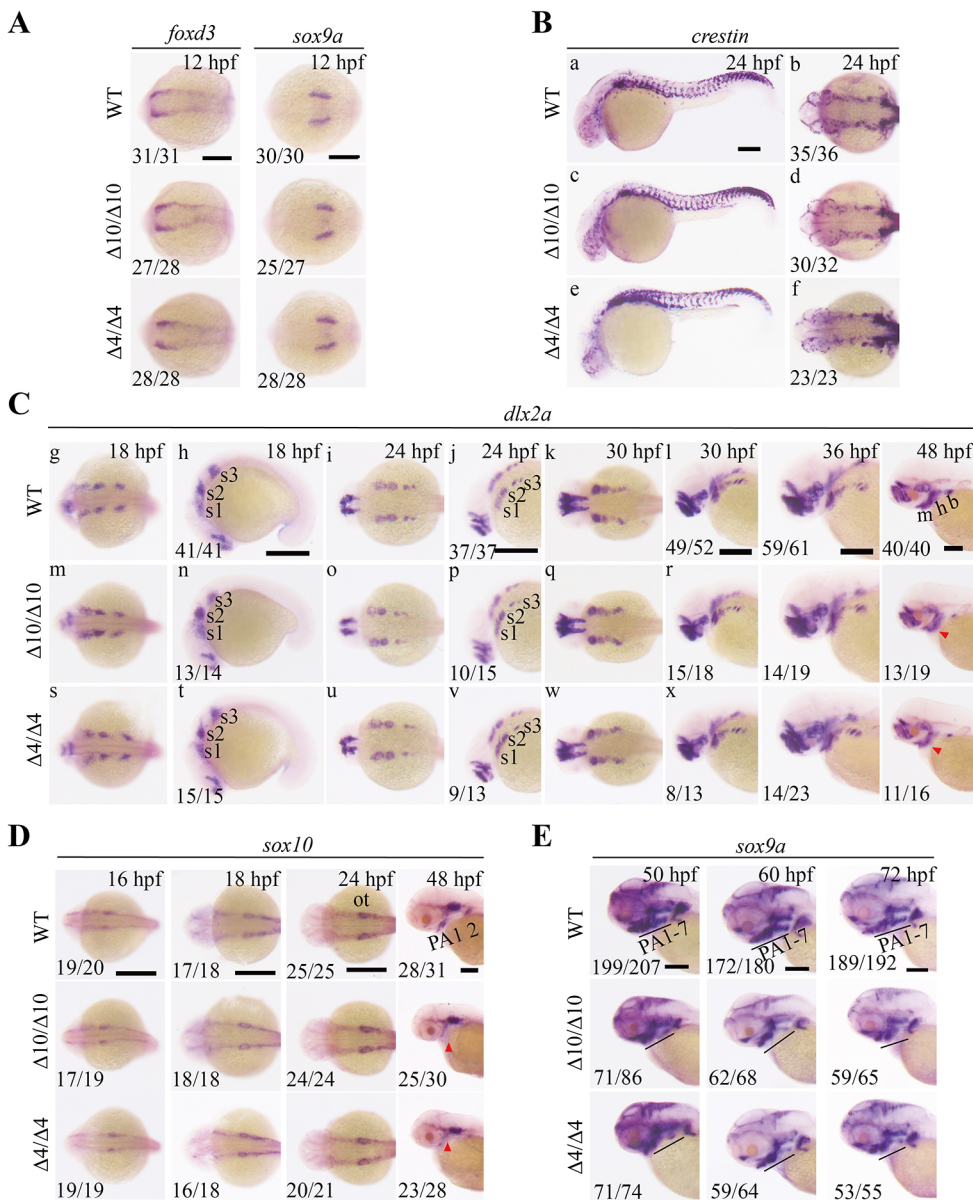


Fig. 2. Genetic deletion of *hspa8* affects pharyngeal arch cartilage development. (A) Expression of early neural crest markers *foxd3* and *sox9a* in WT sibling and *hspa8* mutant embryos ($\Delta 10$ and $\Delta 4$, see Fig. 1A) at 12 hpf. Dorsal views with anterior to the left side. (B) Expression of *crestin* in WT sibling and *hspa8* mutant embryos at 24 hpf. Panels a, c, and e show lateral views, whereas panels b, d, and f show top views. (C) The migration pattern of cranial NCC marker *dlx2a* in WT siblings and *hspa8* mutants. Panels g, i, k, m, o, q, s, u, and w show top views, whereas panels h, j, l, n, p, r, t, v, and x show lateral views. *dlx2a* expression was reduced in the PAs (red arrowheads) of mutant embryos. (D) Expression of *sox10* in WT siblings and *hspa8* mutants. *sox10* expression was reduced in the PAs (red arrowheads) of mutant embryos. Dorsal or lateral views with anterior side to the left. (E) Expression of *sox9a* in WT siblings and *hspa8* mutants. Lateral views with anterior side to the left. s1–s3, neural crest streams 1–3; b, branchial arches; h, hyoid arch; m, mandibular arch; ot, otic vesicle; PA, pharyngeal arch. Scale bars: 200 μ m. The proportion of embryos with the indicated phenotypes is shown in the bottom left corner of each panel.

rescue pharyngeal defects in *hspa8* mutants. Collectively, these results indicate that p53 activation is unlikely to be a major driver of PA defects in *hspa8* mutants.

Inactivation of p53 alleviates Hspa8 depletion-induced p53 signaling enhancement

Unlike WT zebrafish embryos, $p53^{M214K/M214K}$ mutant embryos lack the DNA damage-induced upregulation of some downstream target genes because $p53^{M214K}$ is a non-functional transactivation protein (Berghmans et al., 2005). To further investigate the p53-dependent responses in zebrafish *hspa8* mutant embryos, we compared the mRNA and protein levels of WT p53 and $p53^{M214K}$. Depletion of Hspa8 significantly increased the transcriptional levels of WT p53, whereas little to only a slight difference was observed in those of $p53^{M214K}$ (Fig. 6A). Likewise, whereas the depletion of Hspa8 dramatically increased WT p53 protein expression levels, this was not observed for $p53^{M214K}$ (Fig. 6B). However, the $p53^{M214K}$ protein expression levels were elevated relative to those of WT p53, suggesting that the transactivation

of non-functional p53 might not be strictly regulated. To confirm these results, we investigated the expression of *ccng1* and $\Delta 113p53$ in $p53^{M214K/M214K}$ mutant embryos after depletion of Hspa8, since both genes were upregulated in the WT p53 background. Indeed, the expression levels of *ccng1* and $\Delta 113p53$ were not increased in $p53^{M214K/M214K}$ mutant embryos (Fig. 6C). Taken together, these data suggest that p53 inactivation alleviates Hspa8 depletion-induced p53 signaling enhancement.

Depletion of Hspa8 triggers endoplasmic reticulum stress and the unfolded protein response

To better understand the relationship between PA deficiency and activation of p53 in *hspa8* mutant embryos, we sought to determine which pathway primarily determines the distinct phenotype and p53 induction. To identify differentially expressed genes between WT sibling and mutant embryos, we carried out RNA-sequencing (RNA-seq) analysis of the PA region in WT sibling and mutant embryos at 48 hpf to obtain transcriptome profiles because expression level of *p53* was significantly induced from 42 to

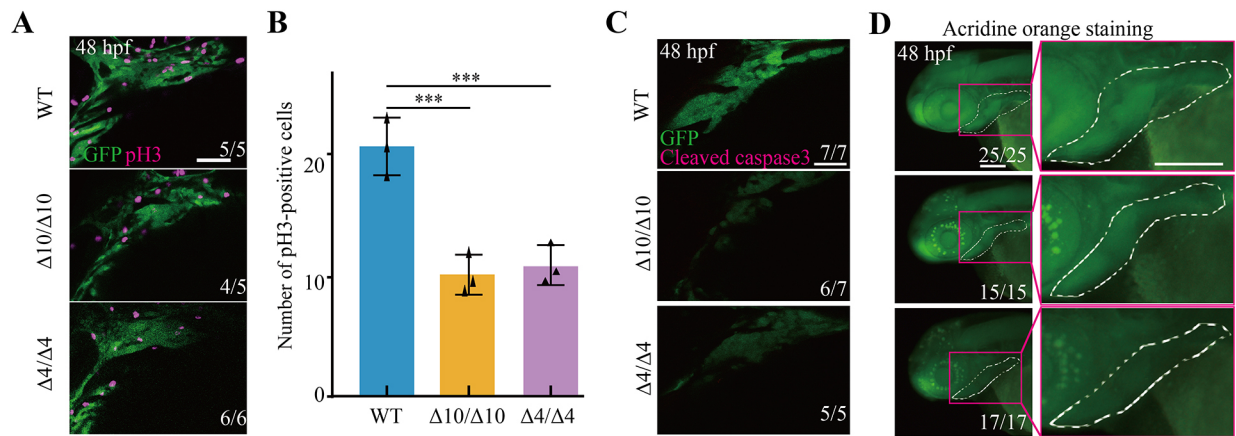


Fig. 3. Depletion of Hspa8 affects the proliferative rather than the apoptotic process in the pharyngeal region. (A) Representative confocal sections of pH3-positive cells in the pharyngeal region of WT siblings and *hspa8* mutants ($\Delta 10$ and $\Delta 4$, see Fig. 1A) at 48 hpf. Embryos with a *Tg(fli1:EGFP)* transgenic background at 48 hpf were immunostained with anti-pH3 antibodies. Scale bar: 50 μ m. (B) Quantitative results from images as shown in A. Values are represented as means \pm s.d. ($n=3$). *** $P<0.001$ (unpaired two-tailed t -test). (C) Representative confocal sections of apoptotic cells in the pharyngeal regions of WT siblings and *hspa8* mutants at 48 hpf. Scale bar: 50 μ m. (D) Acridine Orange staining of WT siblings and *hspa8* mutant embryos at 48 hpf. The dashed lines define the pharyngeal regions. Scale bar: 200 μ m. The proportion of embryos with the indicated phenotypes is shown in the bottom right corner of each panel in A, C and D.

48 hpf (Fig. 7A). In the comparison of transcriptomes between the two genotypes, 390 upregulated and 97 downregulated genes were identified in *hspa8* mutants (Table S1). We noticed that mRNA levels of some Hsp70 family members were induced in *hspa8* mutants at 48 hpf. Among them, *hspa8b* was listed as having significantly higher mRNA levels than the other members (Table S1, Fig. S4B). The qRT-PCR analysis also showed that the mRNA levels of *hspa8b* in PAs were markedly increased in *hspa8* mutants at 48 hpf (Fig. S4C). These results further support that *hspa8*-deleted embryos activate a compensatory network.

All the upregulated genes were annotated with gene ontology (GO) terms and sorted into the ‘biological process’ category. The category ‘amino acid activation/tRNA aminoacylation/tRNA aminoacylation for protein translation’ was listed as the largest class (19/390) (Fig. 7B). The majority of these upregulated genes encode a variety of aminoacyl-tRNA synthetases, which play key roles in protein synthesis (Fig. 7B). Previous studies have shown that activation of ATF4 induces the expression of aminoacyl-tRNA synthetase genes during endoplasmic reticulum (ER) stress (Guan et al., 2014; Han et al., 2013; Krokowski et al., 2013). We noticed that *atf4b* and its target genes, including *atf3*, *ddit3* and *trib3*, as well as other UPR genes (e.g. *atf5a*, *atf6*, *hsp90aa1* and *serpinh1b*) and *p53* were among the upregulated genes (Fig. 7C) (Han et al., 2013). The transcriptional level induction of some genes, such as *atf4b*, *atf3* and *ddit3*, as well as of *atf5a* was further confirmed by qRT-PCR in the PA region of *hspa8* mutant embryos at 48 hpf (Fig. 7D). Taken together, these results suggest that loss of Hspa8 in PA region likely triggers ER stress and the UPR.

The ER plays a role in protein folding, post-translational modification and protein secretion in metazoan cells (Chen and Cubillos-Ruiz, 2021; Ren et al., 2021). The accumulation of unfolded and misfolded proteins in the ER leads to ER stress, which triggers UPR activation to alleviate ER burden and to restore ER homeostasis. The UPR functions are initiated by three ER-localized transmembrane proteins, which relay the cascades through distinct major pathways. These signaling cascades include PERK/p-eIF2 α /ATF4, ATF6, and IRE1-XBP1 (Hetz, 2012; Ron and Walter, 2007; Walter and Ron, 2011; Wang and Kaufman, 2012). Because the transcriptional levels of *atf4b* and its target genes are upregulated in

the PA region after depletion of Hspa8, we next examined the protein level of ATF4 and phosphorylated (activated) eIF2 α . Indeed, both were increased (Fig. 7E), suggesting that the PERK/p-eIF2 α /ATF4 signaling pathway was activated in the PA region after Hspa8 depletion.

Excision of the 26-bp intron from *XBP1* mRNA by unconventional splicing is regarded as an indicator of activation of the IRE1 signaling response to ER stress (Back et al., 2005; Yoshida et al., 2001). We therefore visualized RNA-seq reads mapped to the *xbp1* gene and determined the levels of the altered splicing *xbp1* isoform by semi-quantitative RT-PCR. Although the mRNA level of *xbp1* was increased, the *xbp1* transcripts appeared to be unspliced (Fig. 7F,G). These results suggested that Ire1-Xbp1 signaling pathway likely does not function as a major response pathway. Activation of PERK/p-eIF2 α /ATF4 facilitates the transcription of *ATF6* (Teske et al., 2011). The transcriptional levels of *atf6* were also increased in the PAs of *hspa8* mutant embryos at 48 hpf (Fig. 7C). Collectively, these data indicate that depletion of Hspa8 induces ER stress and the UPR, in which PERK/p-eIF2 α -ATF4 likely functions as the major activated pathway.

Inhibition of PERK/p-eIF2 α /ATF4 activity counteracts the effects of Hspa8 depletion in zebrafish embryos

If activation of the PERK/p-eIF2 α /ATF4 signaling cascade is a major contributor to the reduction in cell proliferation and induction of p53 signaling in PAs after depletion of Hspa8, inhibition of PERK/p-eIF2 α /ATF4 signaling would be expected to restore the development of PAs. To investigate this hypothesis, we used a PERK/p-eIF2 α /ATF4-specific inhibitor, integrated stress response inhibitor (ISRIB), to treat *hspa8*^{-/-} homozygous embryos from 24 to 96 hpf (Sidrauski et al., 2013). As expected, treatment with ISRIB significantly restored normal development of PAs, pectoral fins and eyes (Fig. 8A,B). Likewise, inhibiting PERK/p-eIF2 α /ATF4 activity with ISRIB also rescued the reduced expression of the NCC marker gene *sox9a* in *hspa8* mutant embryos at 96 hpf (Fig. 8C). Similar results were observed in the Alcian Blue-stained cartilage of *hspa8* mutant embryos at 96 hpf after ISRIB treatment (Fig. 8D,E). The rescuing of PA deficiency phenotypes on ISRIB treatment was also

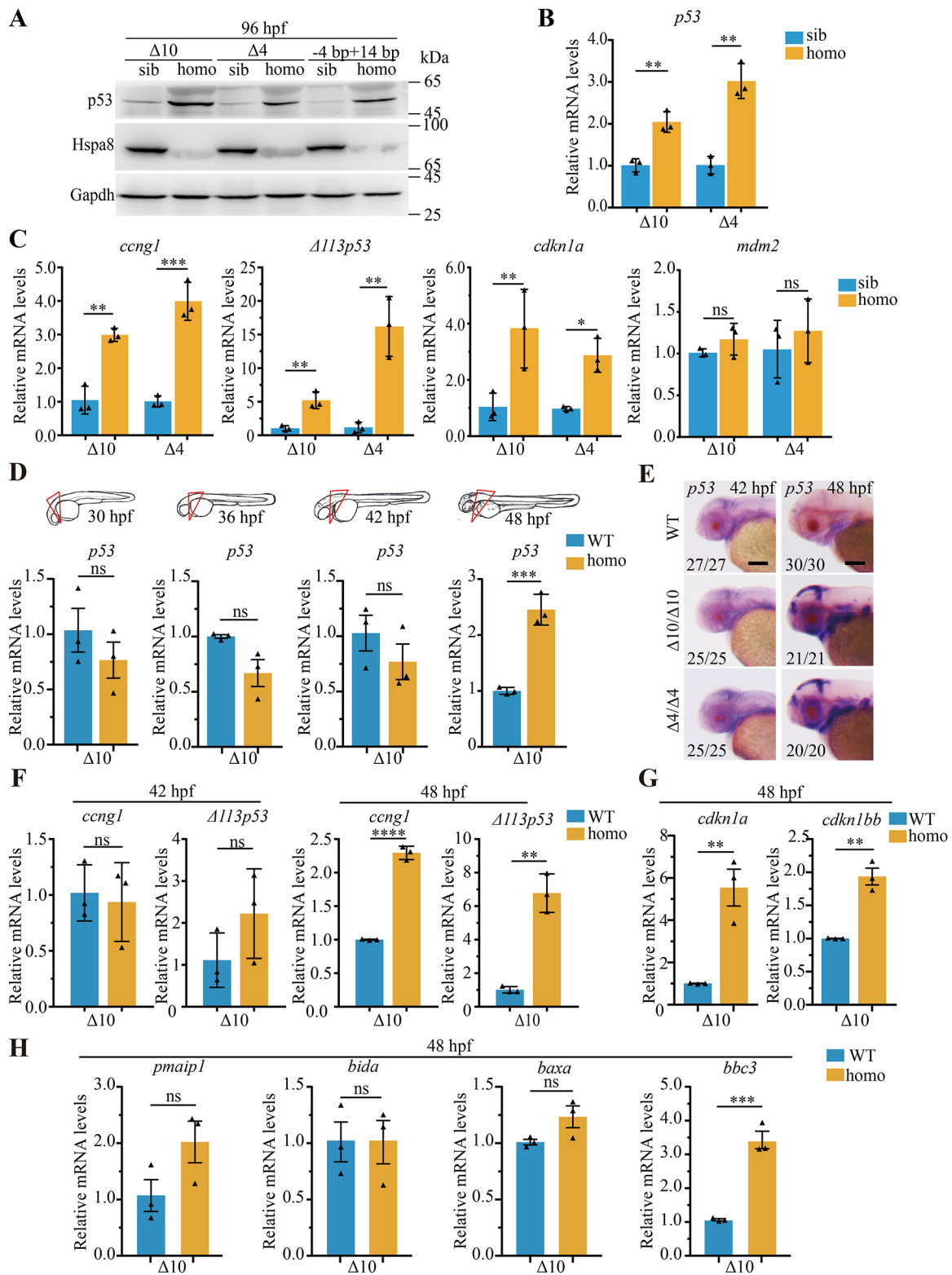


Fig. 4. See next page for legend.

observed at 96 hpf in *hspa8* mutant embryos with a *Tg(fli1:EGFP)* transgenic background (Fig. 8F). Additionally, ISRIB treatment gradually increased the inhibitory effect on the induced *p53* mRNA levels in *hspa8* mutant embryos at 48 and 96 hpf (Fig. 8G), suggesting that inhibition of Perk/p-eIF2 α /Atf4 pathway reduces Hspa8 depletion-induced *p53* activity. To further confirm that the

rescuing effects of ISRIB treatment are a result of a reduced UPR response, we examined the protein levels of Atf4 in PAs after mutant embryos were treated by ISRIB from 24 to 96 hpf. Indeed, treatment with ISRIB reduced the Hspa8 depletion-induced increase in protein levels of Atf4 in PAs (Fig. 8H). Taken together, these results suggest that Hspa8 depletion leads to activation of the

Fig. 4. Depletion of Hspa8 upregulates p53 signaling. (A) Protein levels of p53 in WT siblings (sib) and homozygous (homo) *hspa8* mutants ($\Delta 10$, $\Delta 4$ and -4 bp $+14$ bp, see Fig. 1A) at 96 hpf. *Gapdh* was used as a loading control. Similar results were obtained from three experiments. (B) Expression levels of *p53* mRNA in WT siblings and *hspa8* mutants at 96 hpf, as indicated by qRT-PCR analysis. Values are represented as means \pm s.d. ($n=3$). (C) Expression levels of *p53* target genes in siblings and *hspa8* mutants at 96 hpf. Transcriptional levels of indicated genes were determined using qRT-PCR. Values are represented as means \pm s.d. ($n=3$). (D) The transcriptional levels of *p53* in the PA region of WT sibling and *hspa8* mutant embryos at the indicated developmental stages. The PA region was manually dissected, genotyped and subjected to qRT-PCR analysis. Values are represented as means \pm s.d. ($n=3$). (E) Expression of *p53* in WT sibling and *hspa8* mutant embryos at 42 and 48 hpf. Lateral views with anterior side to the left. Scale bars: 200 μ m. The proportion of embryos with the indicated phenotypes is shown in the bottom left corner of each panel. (F–H) Expression levels of *p53* target genes in the PA region of WT siblings and *hspa8* mutants at indicated developmental stages. The PA region was manually dissected, genotyped, and subjected to qRT-PCR analysis. Values are represented as means \pm s.d. ($n=3$). * $P<0.05$; ** $P<0.01$; *** $P<0.001$; **** $P<0.0001$; ns, not significant (unpaired two-tailed *t*-test).

Perk/p-eIF2 α /Atf4 signaling pathway, resulting in p53 activation as well as aberrant development of PAs.

DISCUSSION

In the present study, we showed that genetic deletion of *hspa8* in zebrafish embryos resulted in aberrant formation of PAs with concomitant reduction of the head, eyes and pectoral fins. Although Hspa8 disruption decreased the level of cell proliferation, it had little effect on apoptosis in the PA region. Furthermore, we observed that Hspa8 depletion led to p53 signaling elevation. However, inactivation of p53 did not rescue the PA reduction associated with *hspa8* mutants despite alleviating Hspa8 depletion-induced p53 signaling. We found that Hspa8 depletion triggers ER stress and then activates the UPR Perk/p-eIF2 α /Atf4 signaling pathway, thereby elevating p53 signaling. Inhibition of the Perk/p-eIF2 α /Atf4 signaling cascade reduced the induced p53 activation and led to significant recovery in the aberrant development of PAs, pectoral fins and eyes in Hspa8-depleted embryos. Overall, our findings reveal the essential role of Hspa8 in zebrafish embryos.

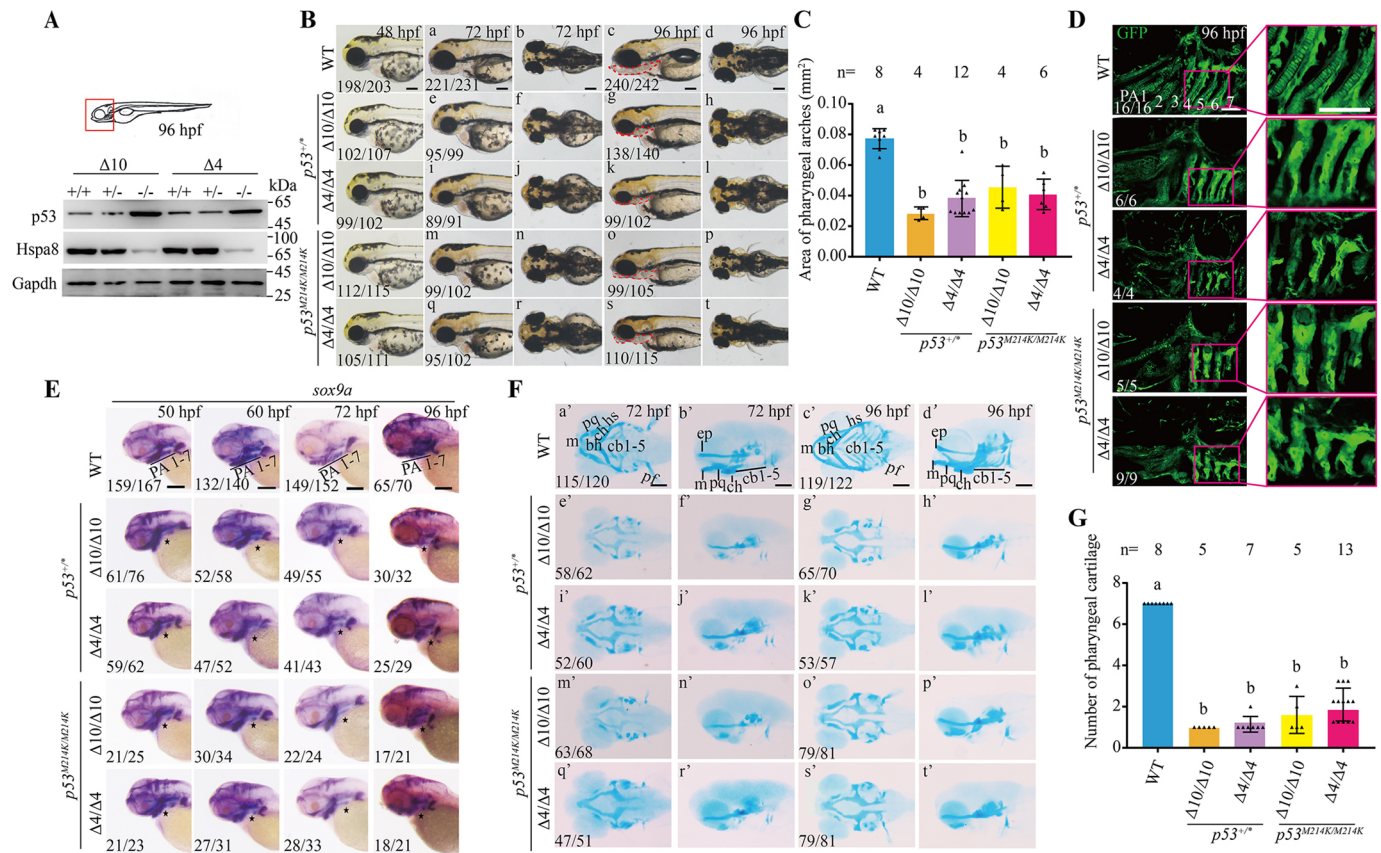


Fig. 5. Inactivation of p53 does not rescue deficiency of pharyngeal arches caused by *hspa8* deletion. (A) Western blotting analysis of the p53 protein level in embryos at 96 hpf with each indicated genotype ($\Delta 10$ and $\Delta 4$, see Fig. 1A). Anterior structures (red box) were manually dissected and subjected to western blotting analysis after embryos were genotyped. Similar results were obtained from three biological replicates. (B) Representative phenotypes of the indicated genotypes (with *p53*^{+/+} indicating *p53*^{+/+} or *p53*^{IM214K}). The dashed lines define the pharyngeal regions. Scale bar: 200 μ m. (C) Quantitative results of the area of pharyngeal regions of embryos at 96 hpf for the indicated genotypes as shown in B. (D) Representative confocal sections showing PA structures of indicated genotyped embryos with a *Tg(fli1:EGFP)* transgenic background at 96 hpf. Scale bars: 50 μ m. (E) *sox9a* expression patterns as detected using whole-mount *in situ* hybridization. Black asterisks indicate absent PAs in mutants. Scale bars: 200 μ m. (F) Alcian Blue-stained head cartilage and PA cartilage. m, Meckel's cartilage; hs, hyosymplectic; bh, basihyal; ch, ceratohyal; pq, palatoquadrate; cb, ceratobranchial; pf, pectoral fin; ep, ethmoid plate. Scale bars: 200 μ m. (G) Quantitative results of the number of pharyngeal cartilages shown in F. Values are represented as means \pm s.d. Groups labeled with different letters are significantly different from each other ($P<0.05$; one-way ANOVA followed by Tukey's post-hoc test). The proportion of embryos with the indicated phenotypes is shown in the bottom left corner of each panel for B, D, E and F.

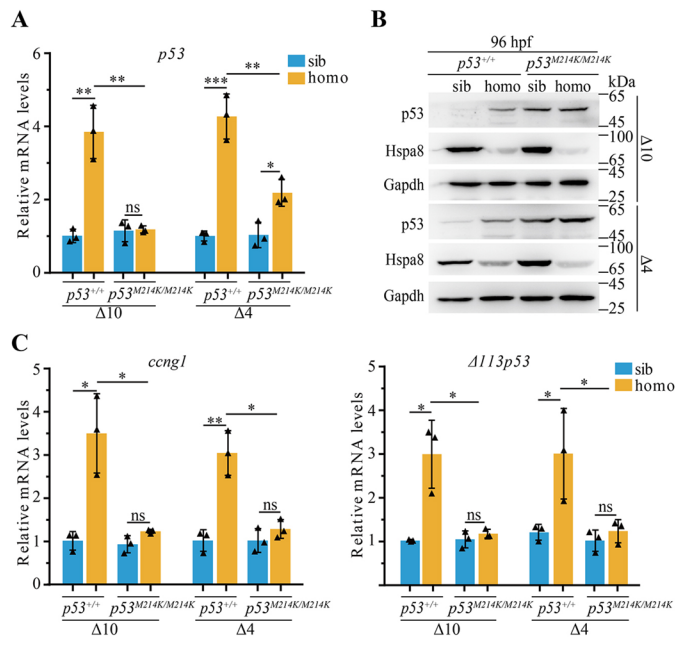


Fig. 6. Inactivation of p53 protein alleviates the effects on Hspa8 depletion-induced p53 signaling. (A) The p53 expression levels in zebrafish embryos with indicated genotypes ($\Delta 10$ and $\Delta 4$, see Fig. 1A) at 96 hpf. The mRNA levels were determined using qRT-PCR. Values are represented as means \pm s.d. ($n=3$). (B) Protein levels of p53 in zebrafish embryos with indicated genotypes at 96 hpf. Gapdh was used as a loading control. Similar results were obtained from three experiments. (C) Expression levels of *ccng1* and $\Delta 113p53$ in zebrafish embryos with indicated genotypes at 96 hpf. The sib and homo labels refer to $\Delta 10$ and $\Delta 4$. Values are represented as means \pm s.d. ($n=3$). * $P<0.05$; ** $P<0.01$; *** $P<0.001$; ns, not significant (unpaired two-tailed *t*-test).

In this study, we used a CRISPR/Cas9 knockout approach and zebrafish as the model organism to investigate the developmental role of *hspa8*. Although HSPA8 is involved in multiple processes (Bonam et al., 2019; Stricher et al., 2013), we observed that genetic deletion of *hspa8* only results in tissue-selective effects during embryonic development. These observations raise an interesting question about a rather tissue-specific defect in what is thought to be a universally required constitutively expressed protein. In WT zebrafish embryos, these specific regions are enriched with *hspa8* transcripts at later developmental stages, which is consistent with the defects observed in *hspa8* mutants. A possible explanation is that there are tissue-specific requirements for Hspa8 during embryogenesis. Additionally, although HSPA8-knockout cells are nonviable, in zebrafish mutant embryos, maternally deposited Hspa8 might first compensate for the lack of the protein; as this protein is gradually turned over throughout embryonic development, the observed phenotypes become more evident. Given that *hspa8* zygotic mutants could not survive to adulthood, we could not obtain maternal-zygotic mutant embryos with eliminated maternally deposited mRNA or protein to evaluate the effects of the complete loss of Hspa8. The contribution of maternally deposited mRNA or protein might explain the genetic deletion of *hspa8* affecting the late but not early stages of PA cartilage development. In addition, genetic deletion of *hspa8* likely induces the activation of a compensatory network, which might compromise the phenotype after *hspa8* was deleted.

Increased mRNA levels of p53 and its target genes have been reported in an *hspa8*^{shi138Tg} mutant line, which contains a disrupted promoter from a retroviral-mediated insertional mutagenesis

(Amsterdam et al., 2004; Danilova et al., 2010). This supports the finding that disruption of Hspa8 in zebrafish embryos leads to induction of p53 activation. We did not find that inactivation of p53 rescued the PA deficiency caused by Hspa8 depletion. This suggests that elevated p53 signaling likely does not contribute to Hspa8 depletion-induced PA deficiency. In contrast, the eye and pectoral fins in *hspa8* mutant embryos were partially rescued by inactivation of p53. The distinct rescuing effects seen upon inactivation of p53 suggest that Hspa8 depletion-induced p53 signaling has different effects in various tissues. These distinct effects of p53 action need further investigation. It should be mentioned that the effect of Hspa8 depletion on increased p53 protein level in zebrafish is different from the effect of HSPA8 reported in cultured HeLa cells (Rohde et al., 2005); in HeLa cells, knockdown of HSPA8 with siRNA has little effect on the p53 protein level (Rohde et al., 2005). Future studies will be needed to determine whether the different roles of Hspa8/HSPA8 are related to cell type.

p53 is a stress response factor and commonly activated upon stress stimuli. The activity of p53 is governed by a variety of distinct regulators (Kastenhuber and Lowe, 2017). Recent studies have identified *hspa8* as a direct p53 target gene in both cultured cells and zebrafish embryos (Mandriani et al., 2016; Mirza et al., 2003). In addition, multiple studies have indicated that HSPA8 and p53 are part of the same complex. HSPA8 likely masks the p53 nuclear localization signal, resulting in the cytoplasmic retention of p53 (Akakura et al., 2001; King et al., 2001). Deficiency of cell-essential genes frequently upregulates p53 signaling (Calo et al., 2018; Danilova et al., 2010). Given the multifaceted roles of HSPA8, the underlying molecular mechanism of the interaction between Hspa8 and p53 signaling was further explored. We narrowed our sights on PA deficiency and used RNA-seq analysis as an unbiased assessment to identify differentially expressed genes in WT sibling and *hspa8* mutant embryos. Hspa8 depletion triggers ER stress and activates a branch of the UPR signaling pathway, the Perk/p-eIF2 α /Atf4 signaling pathway, thus resulting in a tissue-selective phenotype and p53 induction. In support of this view, addition of a specific chemical inhibitor of the Perk/p-eIF2 α /Atf4 signaling pathway abolished the induced p53 activation and rescued PA deficiency in *hspa8* mutant embryos. It should be mentioned that Perk/p-eIF2 α /Atf4 signaling functions as a master signaling pathway but it is likely that is not only pathway involved in this process because the phenotypes in mutant embryos were significantly but not fully rescued. Future studies are needed to elucidate additional signaling mechanisms.

In conclusion, here we show that depletion of Hspa8 in zebrafish embryos induces tissue-specific deficiency, which triggers ER stress and activation of a branch of the UPR signaling pathway, Perk/p-eIF2 α /Atf4 signaling, thus resulting in developmental deficiency of PA (Fig. 8I). Overall, our findings have uncovered an essential role for Hspa8 in zebrafish development and elucidated the underlying mechanism. These findings deepen our understanding of HSPA8 dysregulation and its contribution to the maintenance of cell homeostasis. Importantly, our findings provide a unique *hspa8*-deficient animal model for the *in vivo* evaluation of specific selectivity of chemical compounds targeting HSPA8 for therapeutic application.

MATERIALS AND METHODS

Antibodies and reagents

Primary antibodies used were against: HSPA8 (HSC70) [B-6, 1:1000; sc-7298; Santa Cruz Biotechnology (Santa Cruz, CA, USA)]; histone H3.1

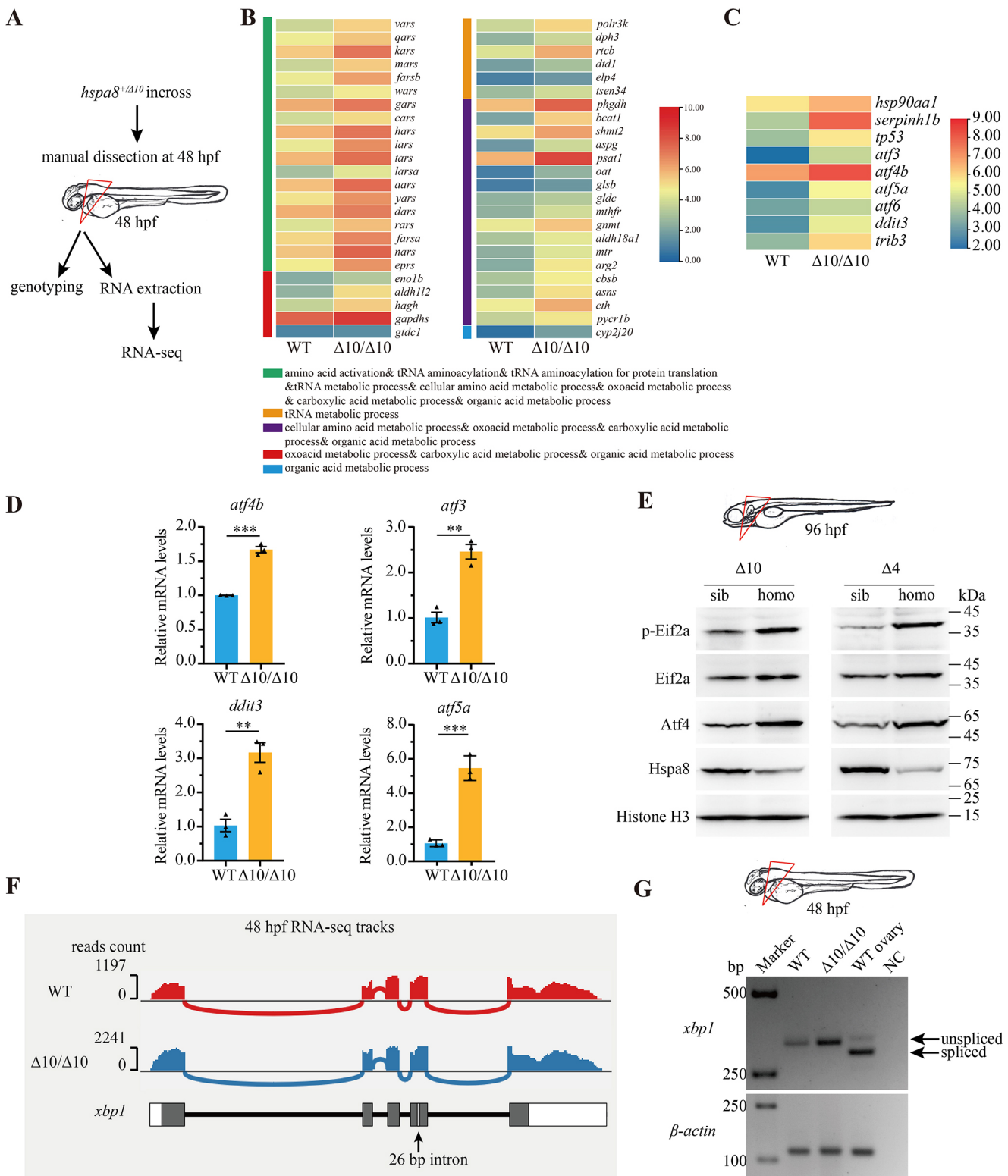


Fig. 7. See next page for legend.

(1:1000; P30266; Abmart (Shanghai, China)); β -tubulin (1:1000; 2146), phospho-histone H3 (Ser10) (D2C8, 1:1000; 3377), ATF-4 (D4B8, 1:1000; 11815), eIF2 α (1:1000; 9722), phospho-eIF2 α (Ser51) (119A11, 1:1000; 3597), and cleaved caspase-3 (Asp175) (5A1E, 1:500; 9664) [all Cell Signaling Technology (Danvers, MA, USA)]; p53 [1:200; ab77813; Abcam (Cambridge, UK)]; GAPDH (1:5000; D110016) and GFP (1:1000, D110008) were [both BBI Life Sciences (Crumlin, UK)]; and collagen

type II (Col2) [1:150; II-II6B3; Developmental Studies Hybridoma Bank (Iowa City, IA, USA)]. DIG-UTP and anti-digoxigenin (DIG)-AP were purchased from Roche (Indianapolis, IN, USA). KOD DNA polymerase and KOD Plus DNA polymerase were purchased from Toyobo (Osaka, Japan). The restriction enzymes Eco147I (FD0424) and T7 Endo I (M0302) were purchased from Thermo Fisher Scientific (Carlsbad, CA, USA) and New England Biolabs (Ipswich, MA, USA), respectively. ISRIB (S0706) and

Fig. 7. Depletion of Hspa8 triggers ER stress and induces activation of the Perk/p-eIF2 α /Atf4 UPR signaling cascade. (A) Schematic representation of the experimental design for the RNA sequencing (RNA-seq) approach. Progeny of *hspa8*^{+/-} fish incrosses were raised to 48 hpf and subjected to genotyping. RNA extraction was performed on manually dissected PAs of embryos (indicated by the red triangle). (B) Heatmaps of transcripts showing the expression-upregulated genes in *hspa8* mutants determined by gene ontology (GO) enrichment analysis. (C) Heatmaps of transcripts showing the expression of indicated genes in *hspa8* mutant zebrafish. Heatmaps in B, C show results from two repeats. (D) Relative expression of the indicated genes in the PAs of WT sibling and *hspa8* mutant embryos at 48 hpf, as indicated by qRT-PCR analysis. Values are represented as means \pm s.d. (n=3). **P<0.01; ***P<0.001 (unpaired two-tailed t-test). (E) Western blotting analysis of the indicated protein levels of the PA region in sibling and *hspa8* mutant embryos at 96 hpf. Similar results were obtained from three biological replicates. PAs were manually dissected and subjected to western blotting analysis after embryos were genotyped. (F) RNA-seq reads mapped to the *xbp1* gene. Coverage tracks are displayed for WT sibling and *hspa8* mutant embryos at 48 hpf. The 26-bp alternative intron related to the UPR is marked on the *xbp1* gene track. (G) The splicing of *xbp1* was determined by RT-PCR analysis. The *xbp1* spliced isoform from the mRNA of adult WT fish ovaries was used as an indicator. β -actin levels were used as an internal control. Similar results were obtained from three biological replicates.

ISRIB (trans-isomer) (S7400) were purchased from Selleck Chemicals (Houston, TX, USA).

Plasmid construction

The plasmids pCS2-Hspa8-GFP and pCS2-Hspa8b-GFP were generated by amplifying the full open reading frame (ORF) of the target gene from cDNA using PCR and subcloned into pCS2-eGFP (a gift from Dr Cumming Duan, University of Michigan, Ann Arbor, USA). The plasmids pCS2-*hspa8* and pCS2-*hspa8b* containing the ORF and the 3' untranslated region of the zebrafish target gene were generated as the positive controls with the following primers: *hspa8* ORF forward, 5'-CCCATCGATGCCAC-CATGTCCAAGGGACCAGCTGTTGG-3'; *hspa8* UTR reverse, 5'-TGCTCTAGAGGGGAATAAGTCACCATTTTATTCTTGTGTC-3' and *hspa8b* ORF forward, 5'-CCGCTCGAGGCCACCATGTCAAAGGGACCAGCA-GTTGGC-3'; *hspa8b* UTR reverse, 5'-TGCTCTAGAGAACAGCAAAGT-CCTTATTGTGCATG-3'.

Cell culture and transfection

The HEK293T cell line was obtained from the American Type Culture Collection (ATCC; Manassas, VA, USA) and authenticated with short tandem repeat profiling by ShCell-Bank (Shanghai, China). Cells were cultured in DMEM (Hyclone, SH30243.01) supplemented with 10% (v/v) FBS and 1% (v/v) penicillin/streptomycin in a humidified chamber with 5% CO₂ at 37°C. Potential contamination by mycoplasmas in cultured cells was tested by use of the EZ-PCR Mycoplasmas Detection Kit (BI, Kibbutz Beit-Haemek, Israel) every 3 months. Plasmids were transfected in 3.5 cm diameter dishes by using 5 μ g polyethylenimine (#23966-2; Polysciences, Warrington, PA, USA). Cells were harvested at 24 h after transfection and then subjected to western blot analysis.

Experimental animals

The Tübingen WT zebrafish (*Danio rerio*), *p53*-defective mutant zebrafish *tp53*^{M214K}, and *Tg (fli1:EGFP)*^{v1} transgenic zebrafish (obtained from Dr Jingxia Liu, Huazhong Agricultural University, China) were raised at 28.5°C and maintained in a 14 h light/10 h dark cycle. Embryos were staged according to standard methods (Kimmel et al., 1995). All protocols were approved and conducted in accordance with the Ethical Committee of the Experimental Animal Care, Ocean University of China.

Generation of *hspa8* mutants

Zebrafish *hspa8* mutants were generated using the CRISPR/Cas9 system. Guide RNAs (gRNAs) were designed using the CRISPR design tool CRISPOR (<http://crispor.tefor.net/crispor.py>). The *hspa8* targeting sequences in the second exon (5'-GTCCAAGGGACCAGCTGT-3') and

third exon (5'-GGAAATTGCTGAGGCCTACC-3') were targeted. The gRNA and Cas9 protein were prepared as previously described and co-injected at the one-cell stage in WT embryos (Rong et al., 2017). The adult F0 fishes were outcrossed with WT fish to obtain the F1 generation, which was genotyped and confirmed by sequencing of targeting sites. For genotyping analysis, genomic DNA was isolated and used as a template for amplification of gRNA targeted sequences with the forward primers 5'-TGACGCACATCCGCATATGC-3' and 5'-GCCCTCTAACTGTGTA-TATG-3' and reverse primers 5'-CAAAGACTGTGTTGGTGGGGTT-3' and 5'-CCTGTCTTTGAGAGTCGTT-3'. PCR products were digested using the restriction enzymes Eco147I or T7 Endo I. To exclude off-target effects, the heterozygous F1 zebrafish were outcrossed with WT zebrafish for two generations. Then, the heterozygous adult fish were increased to obtain embryos for phenotypic analysis. The *hspa8* and *p53* double mutant strains and *hspa8* mutants with a *Tg(fli1:EGFP)*^{v1} genetic background were obtained through natural crossing.

RNA extraction and RT-PCR analysis

Total RNA was extracted from groups of 10 whole zebrafish embryos or manually dissected PAs at indicated stages using the RNAiso Plus kit (Takara Bio, Shiga, Japan), and 2.0 μ g of total RNA was used as a template for reverse transcription. The cDNA was reverse-transcribed using an All-In-One 5X RT MasterMix Kit (Abm, Beijing, China). The cDNA was diluted 10 times as the template. The RT-PCR was carried out with 25 cycles. RT-PCR was performed using Taq DNA polymerase (Takara Bio) with the following primers: *hspa8*-RT-forward, 5'-TGTTGC-CCTCTGTTGTTGAACT-3'; *hspa8*-RT-reverse, 5'-AAGTCACCATTT-TATTCTTGTGTC-3'; *hspa8b*-RT-forward, 5'-GAGGAGGCTTTCCTG-GAGCAGG-3'; *hspa8b*-RT-reverse, 5'-CAGCTACATATCAACCTGA-TAAT-3'; *xbp1*-RT forward, 5'-GTGAGCGATTTAGGTTT-3'; *xbp1*-RT reverse, 5'-TTCATTAAGGGCTTCCAG-3'; β -actin-RT forward, 5'-ACAGGAAAAGATGACACAG-3'; and β -actin-RT reverse, 5'-AGA-GTCCATCACGATACCAG-3'. qRT-PCR was performed using an iCycler iQ Multicolor Real-time PCR Detection System (Bio-Rad Laboratories, Hercules, CA, USA). The primer sequences of zebrafish *atf4b*, *atf3*, *ddit3*, *atf5a* as well as full-length *p53* and its target genes, $\Delta 113p53$, *mdm2* and *ceug1*, as well as *cdkn1a*, *cdkn1bb*, *bida*, and *bbc3* were used as previously described (Boglev et al., 2013; Chen et al., 2005; Essers et al., 2015; Hou et al., 2017; Jiang et al., 2008; Miao et al., 2017; Qi et al., 2021). The following primers were also used: *baxa* forward, 5'-GGCTATTTCAAC-CAGGGTTC-3'; *baxa* reverse, 5'-TGCGAATCACCAATGCTGT-3'; *pmaip1* forward, 5'-ATGGCGAAGAAAGAGCAAAC; *pmaip1* reverse, 5'-CTCATCGCTTCCCTCCATT; *hspa8b* forward, 5'-TCAGAGGTG-TAATCAGCCAG-3'; and *hspa8b* reverse, 5'-GAACAGCAAAGTCTT-TATTGTGTCATG-3'. The mRNA levels of the genes of interest were calculated using the 2^{- $\Delta\Delta$ Ct} method and normalized to β -actin levels.

Whole-mount *in situ* hybridization

WISH using a DIG-labeled RNA riboprobe was performed as previously described (Bai et al., 2014). Zebrafish embryos at different stages were fixed in 4% paraformaldehyde (PFA) overnight before being processed for WISH analysis. DIG-UTP-labeled antisense RNA probes for *p53*, *sox9a*, *sox10*, *foxd3*, *dlx2a* and *crestin* were generated and used for WISH analysis. The plasmid DNA containing a partial ORF and the 3' untranslated region of zebrafish *hspa8* was used to generate sense and antisense riboprobes. Images were captured using a Leica M205 microscope (Leica Microsystems, Wetzlar, Germany).

Alcian Blue staining

Alcian Blue staining was performed as previously described (Li et al., 2018). Zebrafish embryos were fixed in 4% paraformaldehyde (PFA) overnight at 4°C. After fixation, the embryos were washed with PBS for 10 min. Embryos were then stained with Alcian Blue staining buffer (0.15% Alcian Blue, 80% ethanol, and 20% acetic acid; A600298, Sangon Biotech, Shanghai, China) at room temperature for 90 min. Next, the embryos were rehydrated through a graded series of alcohols to distilled water and then treated with 50 mg/ml trypsin in supersaturated borax at room temperature until the tissues were soft enough to dissect. Next, the embryos were

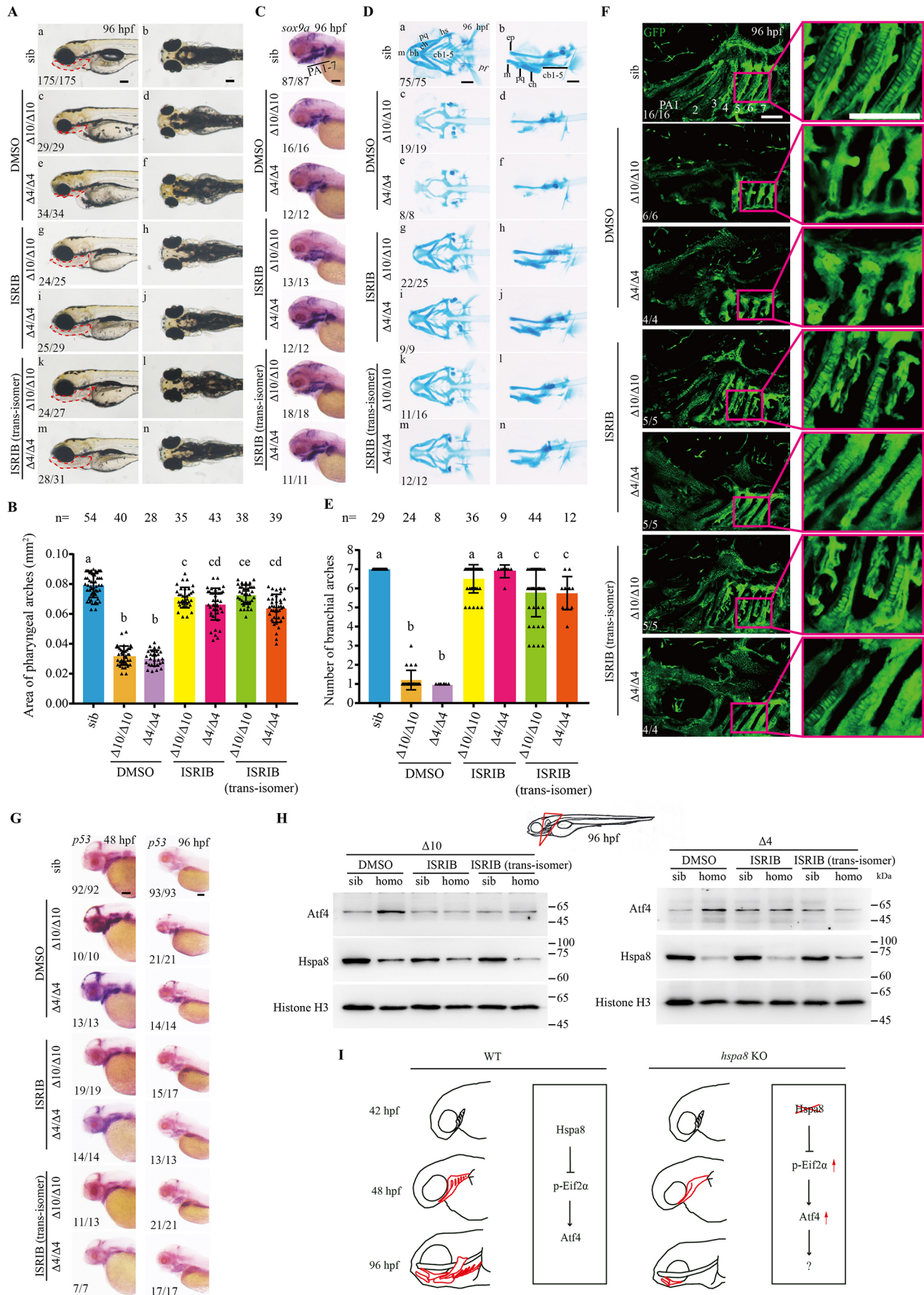


Fig. 8. See next page for legend.

Fig. 8. Pharmacological inhibition of Perk/p-eIF2 α /Atf4 signaling counteracts the effects of Hspa8 depletion in zebrafish embryos.

(A) Representative images of WT sibling and *hspa8* mutant embryos ($\Delta 10$ and $\Delta 4$, see Fig. 1A) at 96 hpf treated with or without ISRIB or ISRIB (trans-isomer). Scale bar: 200 μ m. (B) Quantitative results of the area of pharyngeal regions for embryos shown in A. (C) Expression of *sox9* in WT sibling and *hspa8* mutant embryos at 96 hpf treated with or without ISRIB or ISRIB (trans-isomer). Scale bar: 200 μ m. (D) Representative images of Alcian Blue-stained head cartilage and pharyngeal arch cartilage in WT sibling and *hspa8* mutant embryos shown in A. Scale bar: 200 μ m. m, Meckel's cartilage; hs, hyosymplectic; bh, basihyal; ch, ceratohyal; pq, palatoquadrate; cb, ceratobranchial; pf, pectoral fin; ep, ethmoid plate. (E) Quantitative results of the number of pharyngeal cartilages shown in D. (F) Representative confocal images of WT sibling and *hspa8* mutant embryos with a *Tg(fli1:EGFP)* transgenic background at 96 hpf treated with or without ISRIB or ISRIB (trans-isomer). Scale bars: 50 μ m. (G) Expression of *p53* in WT sibling and *hspa8* mutant embryos at 48 and 96 hpf treated with or without ISRIB or ISRIB (trans-isomer). Scale bars: 200 μ m. (H) Treatment with ISRIB or ISRIB (trans-isomer) impeded Hspa8 depletion-induced Atf4 protein levels in PAs. Similar results were obtained from three experiments. Progenies of *hspa8*^{+/-} (A, C, D, G, H) or *hspa8*^{+/-}; *Tg(fli1:EGFP)* (F) incrosses were raised to 24 hpf and treated with 600 μ M ISRIB or ISRIB (trans-isomer) from 24 hpf to the indicated time points. Embryos were harvested for indicated analyses and genotyped. Values are represented as means \pm s.d. Groups labeled with different letters are significantly different from each other at $P < 0.05$ (one-way ANOVA followed by Tukey's post-hoc test). The proportion of embryos with the indicated phenotypes is shown in the bottom left corner of each panel for A, C, D, F and G. (I) Model illustrating selective developmental deficiency of pharyngeal arches in *hspa8* mutant embryos.

transferred into an 1% KOH solution for 20 min and then washed in distilled water for 5 min. Finally, the embryos were dehydrated with a graded series of glycerol solutions and dissected for imaging. The embryos were imaged using a Leica M205 microscope.

Immunoblots

Immunoblotting was performed as previously described (Wang et al., 2021). Whole embryos and manually dissected anterior structures or PAs from embryos at indicated time points were collected and mixed in each tube, frozen in liquid nitrogen for 2 min, and lysed in RIPA buffer (50 mM Tris-HCl, 150 mM NaCl, 1 mM EDTA, 0.5% NP-40, 0.1% SDS, pH 7.5) with protease inhibitor containing PMSF (1 mM), Bestatin (10 μ M), Pepstatin A (15 μ M), E-64 (14 μ M), Aprotinin (0.8 μ M) and Leupeptin (10 μ M) (BBI Life Sciences, Shanghai, China) at 4°C for 15 min. Next, the samples were heated at 95°C for 5 min and centrifuged to remove the precipitate. Following separation using 10% SDS-PAGE, the proteins were transferred onto PVDF membranes and incubated with primary antibodies overnight at 4°C after being blocked with 5% nonfat milk. Primary antibodies were detected using an HRP-conjugated secondary antibody (Beyotime Biotechnology, Shanghai, China). Full blot images are shown in Fig. S6.

Whole-mount immunofluorescence staining

Whole-mount immunofluorescence staining was performed as previously described (Laguerre et al., 2005; Vihtelic et al., 2001). Briefly, embryos were fixed with 4% PFA overnight at 4°C. After fixation, the embryos were washed in 0.2% Triton X-100 in PBS (PBST) for 10 min and blocked with 5% FBS in PBST with 1% BSA and 1% DMSO added before immunostaining for at least 1 h. Rabbit anti-phospho-histone H3, rabbit anti-cleaved caspase-3, and rabbit anti-Col2 primary antibodies were diluted in the blocking solution and incubated at 4°C overnight. Next, the embryos were washed in PBST, incubated with the secondary antibody anti-rabbit-IgG conjugated to Cy3 or Cy5, and incubated at 4°C overnight. After being washed with PBST, the nuclei were counterstained with DAPI. All samples were imaged using a Leica SP8 confocal or Leica M205 microscope (Leica Microsystems).

AO staining was performed as previously described (Liu et al., 2014). The living embryos were incubated for 30 min in 2 μ g/ml AO (Sigma-Aldrich, St Louis, MO, USA) at room temperature. The embryos were then washed

in distilled water three times and anesthetized with 0.03% tricaine. Images were captured using a Leica M205 microscope.

RNA-seq transcriptome analysis

PA regions from 40 WT siblings or *hspa8* mutants were dissected in biological duplicates, and total RNA was isolated using Trizol according to standard protocols. We performed 2 \times 150 bp paired-end sequencing on an Illumina NovaseqTM 6000 by Lc-Bio following the vendor's recommended protocol (LC-Bio Technology Co., Ltd., Hangzhou, China). For data processing, the reads were mapped to the reference genome index constructed by STAR (version 2.7.8a) using Danio_rerio.GRCz11.104.chr.gtf and Danio_rerio.GRCz11.104.chr.fa. The raw counts of the genes were obtained using featureCounts in the subread version 1.6.1 package. Sample normalization and differential expression analysis were performed using DESeq2. Then, the relative expression level FPKM mapped reads of the differential genes were calculated according to the traditional formula, and a gene expression heatmap was obtained using TBtools (version 1.09852). The RNA-seq data were deposited to the Sequence Read Archive database under accession number SRP350317 (<https://www.ncbi.nlm.nih.gov/sra/PRJNA788011>).

Pharmacological treatments

ISRIB and ISRIB (trans-isomer) were used to inhibit Perk/p-eIF2 α /Atf4 signaling activity. Progenies of *hspa8*^{+/-} or *hspa8*^{+/-}; *Tg(fli1:EGFP)*^{Y1} incrosses were raised to 24 hpf and treated with 600 μ M ISRIB or ISRIB (trans-isomer) from 24 hpf to indicated stages. Embryos were harvested for further analysis and then subjected to genotyping analysis.

Statistical analysis

All experiments were repeated three times. All experimental data were analyzed using GraphPad Prism version 7 (GraphPad, San Diego, CA, USA). Data are presented as mean \pm s.d. Unpaired, two-tailed Student's *t*-tests were used for comparisons between two groups; one-way analysis of variance with Tukey's post-hoc test was used for multiple comparisons, and significance was defined as $P < 0.05$.

Acknowledgements

We thank Dr Jingxia Liu of Huazhong Agricultural University for providing *Tg(fli1:EGFP)*^{Y1} transgenic zebrafish, Dr Bo Zhang of Peking University for providing probes for *in situ* hybridization analysis, and Dr Shan Gao of Ocean University of China for assisting with RNA-seq data analysis.

Competing interests

The authors declare no competing or financial interests.

Author contributions

Conceptualization: C.W., X.Z., X.W., X.R., J.Z.; Methodology: C.W., X.Z., X.W., Y.B., X.R., J.Z.; Software: C.W., X.Z., X.W., Y.Z., M.L., J.P.; Validation: C.W., X.Z., X.W., Y.Z., M.L., J.P., X.R., J.Z.; Formal analysis: C.W., X.Z., X.W., Y.Z., M.L., J.P., X.R., J.Z.; Investigation: C.W., X.Z., X.W., Y.Z., M.L., J.P., X.R., J.Z.; Resources: X.R., J.Z.; Data curation: X.R., J.Z.; Writing - original draft: X.R., J.Z.; Writing - review & editing: X.R., J.Z.; Visualization: C.W., X.Z., X.W., Y.Z., M.L., J.P., X.R., J.Z.; Supervision: X.R., J.Z.; Project administration: X.R., J.Z.; Funding acquisition: X.R., J.Z.

Funding

This work was supported by the Marine S&T Fund of Shandong Province for Pilot National Laboratory for Marine Science and Technology (Qingdao) (No. 2022QNLMO30003 to J.Z. and X.R.), the National Key R & D Program of China (2018YFA0801000 to J.Z.), the National Natural Science Foundation of China (31601863 to X.R., 31872189 and 32170834 to J.Z.), the Natural Science Foundation of Shandong Province (major basic research projects) (ZR2019ZD18 to J.Z. and ZR2021MC075 to X.R.). The funders had no role in study design, data collection and analysis, decision to publish, or preparation of the manuscript.

Data availability

The RNA-seq data were deposited to the Sequence Read Archive database under accession numbers SRP350317 (<https://www.ncbi.nlm.nih.gov/sra/PRJNA788011>).

Peer review history

The peer review history is available online at <https://journals.biologists.com/jcs/lookup/doi/10.1242/jcs.259734.reviewer-comments.pdf>.

References

- Akakra, S., Yoshida, M., Yoneda, Y. and Horinouchi, S. (2001). A role for Hsc70 in regulating nucleocytoplasmic transport of a temperature-sensitive p53 (p53(Val-135)). *J. Biol. Chem.* **276**, 14649-14657. doi:10.1074/jbc.M100200200
- Amsterdam, A., Nissen, R. M., Sun, Z., Swindell, E. C., Farrington, S. and Hopkins, N. (2004). Identification of 315 genes essential for early zebrafish development. *Proc. Natl. Acad. Sci. USA* **101**, 12792-12797. doi:10.1073/pnas.0403929101
- Anderson, R. M., Bosch, J. A., Goll, M. G., Hesselson, D., Dong, P. D. S., Shin, D. H., Chi, N. C., Shin, C. H., Schlegel, A., Halpern, M. et al. (2009). Loss of Dnmt1 catalytic activity reveals multiple roles for DNA methylation during pancreas development and regeneration. *Dev. Biol.* **334**, 213-223. doi:10.1016/j.ydbio.2009.07.017
- Back, S. H., Schröder, M., Lee, K., Zhang, K. and Kaufman, R. J. (2005). ER stress signaling by regulated splicing: IRE1/HAC1/XBP1. *Methods* **35**, 395-416. doi:10.1016/j.ymeth.2005.03.001
- Bai, Y., Tan, X. G., Zhang, H. F., Liu, C. D., Zhao, B. B., Li, Y., Lu, L., Liu, Y. Z. and Zhou, J. F. (2014). Ror2 receptor mediates Wnt11 ligand signaling and affects convergence and extension movements in zebrafish. *J. Biol. Chem.* **289**, 20664-20676. doi:10.1074/jbc.M114.586099
- Berghmans, S., Murphey, R. D., Wienholds, E., Neuberg, D., Kutok, J. L., Fletcher, C. D. M., Morris, J. P., Liu, T. X., Schulte-Merker, S., Kanki, J. P. et al. (2005). tp53 mutant zebrafish develop malignant peripheral nerve sheath tumors. *Proc. Natl. Acad. Sci. USA* **102**, 407-412. doi:10.1073/pnas.0406252102
- Boglev, Y., Badrock, A. P., Trotter, A. J., Du, Q., Richardson, E. J., Parslow, A. C., Markmiller, S. J., Hall, N. E., De Jong-Curtain, T. A., Ng, A. Y. et al. (2013). Autophagy induction is a Tor- and Tp53-independent cell survival response in a zebrafish model of disrupted ribosome biogenesis. *PLoS Genet.* **9**, e1003279. doi:10.1371/journal.pgen.1003279
- Bonam, S. R., Ruff, M. and Muller, S. (2019). HSPA8/HSC70 in immune disorders: a molecular rheostat that adjusts chaperone-mediated autophagy substrates. *Cells* **8**, 849. doi:10.3390/cells8080849
- Calo, E., Gu, B., Bowen, M. E., Aryan, F., Zalc, A., Liang, J. L., Flynn, R. A., Swigut, T., Chang, H. Y., Attardi, L. D. et al. (2018). Tissue-selective effects of nucleolar stress and rDNA damage in developmental disorders. *Nature* **554**, 112-117. doi:10.1038/nature25449
- Chen, X. and Cubillos-Ruiz, J. R. (2021). Endoplasmic reticulum stress signals in the tumour and its microenvironment. *Nat. Rev. Cancer* **21**, 71-88. doi:10.1038/s41568-020-00312-2
- Chen, J., Ruan, H., Ng, S. M., Gao, C., Soo, H. M., Wu, W., Zhang, Z. H., Wen, Z. L., Lane, D. P. and Peng, J. R. (2005). Loss of function of def selectively up-regulates Delta 113p53 expression to arrest expansion growth of digestive organs in zebrafish. *Genes Dev.* **19**, 2900-2911. doi:10.1101/gad.1366405
- Danilova, N., Kumagai, A. and Lin, J. (2010). p53 upregulation is a frequent response to deficiency of cell-essential genes. *PLoS One* **5**, e15938. doi:10.1371/journal.pone.0015938
- Daugaard, M., Rohde, M. and Jäättelä, M. (2007). The heat shock protein 70 family: highly homologous proteins with overlapping and distinct functions. *FEBS Lett.* **581**, 3702-3710. doi:10.1016/j.febslet.2007.05.039
- Dutton, K. A., Pauliny, A., Lopes, S. S., Elworthy, S., Carney, T. J., Rauch, J., Geisler, R., Haffter, P. and Kelsh, R. N. (2001). Zebrafish colourless encodes sox10 and specifies non-ectomesenchymal neural crest fates. *Development* **128**, 4113-4125. doi:10.1242/dev.128.21.4113
- El-Broklosy, M. A., Kontarakis, Z., Rossi, A., Kuenne, C., Gunther, S., Fukuda, N., Kikhi, K., Boezio, G. L. M., Takacs, C. M., Lai, S. L. et al. (2019). Genetic compensation triggered by mutant mRNA degradation. *Nature* **568**, 193-197. doi:10.1038/s41586-019-1064-z
- Eisen, G. E., Choi, L. Y., Millen, K. J., Grinblat, Y. and Prince, V. E. (2008). Zic1 and Zic4 regulate zebrafish roof plate specification and hindbrain ventricle morphogenesis. *Dev. Biol.* **314**, 376-392. doi:10.1016/j.ydbio.2007.12.006
- Essers, P. B., Klason, T. D., Pereboom, T. C., Mans, D. A., Nicastro, M., Boldt, K., Giles, R. H. and Macinnes, A. W. (2015). The von Hippel-Lindau tumor suppressor regulates programmed cell death 5-mediated degradation of Mdm2. *Oncogene* **34**, 771-779. doi:10.1038/onc.2013.598
- Florin, L., Becker, K. A., Sapp, C., Lambert, C., Sirma, H., Müller, M., Streeck, R. E. and Sapp, M. (2004). Nuclear translocation of papillomavirus minor capsid protein L2 requires Hsc70. *J. Virol.* **78**, 5546-5553. doi:10.1128/JVI.78.11.5546-5553.2004
- Guan, B.-J., Krokowski, D., Majumder, M., Schmotzer, C. L., Kimball, S. R., Merrick, W. C., Koromilas, A. E. and Hatzoglou, M. (2014). Translational control during endoplasmic reticulum stress beyond phosphorylation of the translation initiation factor eIF2alpha. *J. Biol. Chem.* **289**, 12593-12611. doi:10.1074/jbc.M113.543215
- Han, J., Back, S. H., Hur, J., Lin, Y.-H., Gildersleeve, R., Shan, J., Yuan, C. L., Krokowski, D., Wang, S., Hatzoglou, M. et al. (2013). ER-stress-induced transcriptional regulation increases protein synthesis leading to cell death. *Nat. Cell Biol.* **15**, 481-490. doi:10.1038/ncb2738
- Hetz, C. (2012). The unfolded protein response: controlling cell fate decisions under ER stress and beyond. *Nat. Rev. Mol. Cell Biol.* **13**, 89-102. doi:10.1038/nrm3270
- Hochgreh-Hagele, T. and Bronner, M. E. (2013). A novel FoxD3 gene trap line reveals neural crest precursor movement and a role for FoxD3 in their specification. *Dev. Biol.* **374**, 1-11. doi:10.1016/j.ydbio.2012.11.035
- Hou, N., Yang, Y., Scott, I. C. and Lou, X. (2017). The Sec domain protein Scfd1 facilitates trafficking of ECM components during chondrogenesis. *Dev. Biol.* **421**, 8-15. doi:10.1016/j.ydbio.2016.11.010
- Hu, Z. L., Holzschuh, J. and Driever, W. (2015). Loss of DDB1 leads to transcriptional p53 pathway activation in proliferating cells, cell cycle deregulation, and apoptosis in zebrafish embryos. *PLoS One* **10**, e0134299. doi:10.1371/journal.pone.0134299
- Jiang, Z., Song, J., Qi, F., Xiao, A., An, X., Liu, N. A., Zhu, Z., Zhang, B. and Lin, S. (2008). Exdpf is a key regulator of exocrine pancreas development controlled by retinoic acid and ptf1a in zebrafish. *PLoS Biol.* **6**, e293. doi:10.1371/journal.pbio.0060293
- Kastenhuber, E. R. and Lowe, S. W. (2017). Putting p53 in context. *Cell* **170**, 1062-1078. doi:10.1016/j.cell.2017.08.028
- Kimmel, C. B., Ballard, W. W., Kimmel, S. R., Ullmann, B. and Schilling, T. F. (1995). Stages of embryonic development of the zebrafish. *Dev. Dyn.* **203**, 253-310. doi:10.1002/aja.1002030302
- King, F. W., Wawrzynow, A., Hohfeld, J. and Zylicz, M. (2001). Co-chaperones Bag-1, Hop and Hsp40 regulate Hsc70 and Hsp90 interactions with wild-type or mutant p53. *EMBO J.* **20**, 6297-6305. doi:10.1093/emboj/20.22.6297
- Krokowski, D., Han, J., Saikia, M., Majumder, M., Yuan, C. L., Guan, B. J., Bevilacqua, E., Bussolati, O., Broer, S., Arvan, P. et al. (2013). A self-defeating anabolic program leads to beta-cell apoptosis in endoplasmic reticulum stress-induced diabetes via regulation of amino acid flux. *J. Biol. Chem.* **288**, 17202-17213. doi:10.1074/jbc.M113.466920
- Laguette, L., Soubiran, F., Ghysen, A., König, N. and Dambly-Chaudière, C. (2005). Cell proliferation in the developing lateral line system of zebrafish embryos. *Dev. Dyn.* **233**, 466-472. doi:10.1002/dvdy.20343
- Lawson, N. D. and Weinstein, B. M. (2002). In vivo imaging of embryonic vascular development using transgenic zebrafish. *Dev. Biol.* **248**, 307-318. doi:10.1006/dbio.2002.0711
- Li, L., Mao, A., Wang, P., Ning, G., Cao, Y. and Wang, Q. (2018). Endodermal pouch-expressed dmt2b is important for pharyngeal cartilage formation. *Biol. Open* **7**, bio035444. doi:10.1242/bio.035444
- Liu, T., Daniels, C. K. and Cao, S. (2012). Comprehensive review on the HSC70 functions, interactions with related molecules and involvement in clinical diseases and therapeutic potential. *Pharmacol. Ther.* **136**, 354-374. doi:10.1016/j.pharmthera.2012.08.014
- Liu, C., Luan, J., Bai, Y., Li, Y., Lu, L., Liu, Y., Hakuno, F., Takahashi, S., Duan, C. and Zhou, J. (2014). Aspp2 negatively regulates body growth but not developmental timing by modulating IRS signaling in zebrafish embryos. *Gen. Comp. Endocrinol.* **197**, 82-91. doi:10.1016/j.ygcen.2013.12.006
- Ma, Z., Zhu, P., Shi, H., Guo, L., Zhang, Q., Chen, Y., Chen, S., Zhang, Z., Peng, J. and Chen, J. (2019). PTC-bearing mRNA elicits a genetic compensation response via Upf3a and COMPASS components. *Nature* **568**, 259-263. doi:10.1038/s41586-019-1057-y
- Mandriani, B., Castellana, S., Rinaldi, C., Manzoni, M., Venuto, S., Rodriguez-Aznar, E., Galceran, J., Nieto, M. A., Borsani, G., Monti, E. et al. (2016). Identification of p53-target genes in Danio rerio. *Sci. Rep.* **6**, 32474. doi:10.1038/srep32474
- Miao, L., Yuan, Y., Cheng, F., Fang, J., Zhou, F., Ma, W., Jiang, Y., Huang, X., Wang, Y., Shan, L. et al. (2017). Translation repression by maternal RNA binding protein Zar1 is essential for early oogenesis in zebrafish. *Development* **144**, 128-138. doi:10.1242/dev.144642
- Minoux, M. and Rijli, F. M. (2010). Molecular mechanisms of cranial neural crest cell migration and patterning in craniofacial development. *Development* **137**, 2605-2621. doi:10.1242/dev.040048
- Mirza, A., Wu, Q., Wang, L., McClanahan, T., Bishop, W. R., Gheyas, F., Ding, W., Hutchins, B., Hockenberry, T., Kirschmeier, P. et al. (2003). Global transcriptional program of p53 target genes during the process of apoptosis and cell cycle progression. *Oncogene* **22**, 3645-3654. doi:10.1038/sj.onc.1206477
- Qi, Z., Yan, D., Cao, L., Xu, Y. and Chang, M. (2021). Zebrafish BID exerts an antibacterial role by negatively regulating p53, but in a Caspase-8-independent manner. *Front. Immunol.* **12**, 707426. doi:10.3389/fimmu.2021.707426
- Ren, J., Bi, Y., Sowers, J. R., Hetz, C. and Zhang, Y. (2021). Endoplasmic reticulum stress and unfolded protein response in cardiovascular diseases. *Nat. Rev. Cardiol.* **18**, 499-521. doi:10.1038/s41569-021-00511-w
- Rohde, M., Daugaard, M., Jensen, M. H., Helin, K., Nylandsted, J. and Jäättelä, M. (2005). Members of the heat-shock protein 70 family promote cancer cell growth by distinct mechanisms. *Genes Dev.* **19**, 570-582. doi:10.1101/gad.305405
- Ron, D. and Walter, P. (2007). Signal integration in the endoplasmic reticulum unfolded protein response. *Nat. Rev. Mol. Cell Biol.* **8**, 519-529. doi:10.1038/nrm2199

- Rong, X., Zhou, Y., Liu, Y., Zhao, B., Wang, B., Wang, C., Gong, X., Tang, P., Lu, L., Li, Y. et al. (2017). Glutathione peroxidase 4 inhibits Wnt/beta-catenin signaling and regulates dorsal organizer formation in zebrafish embryos. *Development* **144**, 1687-1697. doi:10.1242/dev.144261.
- Sen, R., Pezoa, S. A., Carpio Shull, L., Hernandez-Lagunas, L., Niswander, L. A. and Artinger, K. B. (2018). Kat2a and Kat2b acetyltransferase activity regulates craniofacial cartilage and bone differentiation in zebrafish and mice. *J. Dev. Biol.* **6**, 27. doi:10.3390/jdb6040027
- Sidrauski, C., Acosta-Alvear, D., Khoutorsky, A., Vedantham, P., Hearn, B. R., Li, H., Gamache, K., Gallagher, C. M., Ang, K. K., Wilson, C. et al. (2013). Pharmacological brake-release of mRNA translation enhances cognitive memory. *Elife* **2**, e00498. doi:10.7554/eLife.00498
- Sperber, S. M., Saxena, V., Hatch, G. and Ekker, M. (2008). Zebrafish *dlx2a* contributes to hindbrain neural crest survival, is necessary for differentiation of sensory ganglia and functions with *dlx1a* in maturation of the arch cartilage elements. *Dev. Biol.* **314**, 59-70. doi:10.1016/j.ydbio.2007.11.005
- Stricher, F., Macri, C., Ruff, M. and Muller, S. (2013). HSPA8/HSC70 chaperone protein Structure, function, and chemical targeting. *Autophagy* **9**, 1937-1954. doi:10.4161/auto.26448
- Teske, B. F., Wek, S. A., Bunpo, P., Cundiff, J. K., Mcclintick, J. N., Anthony, T. G. and Wek, R. C. (2011). The eIF2 kinase PERK and the integrated stress response facilitate activation of ATF6 during endoplasmic reticulum stress. *Mol. Biol. Cell* **22**, 4390-4405. doi:10.1091/mbc.e11-06-0510
- Van Nostrand, J. L., Brady, C. A., Jung, H. Y., Fuentes, D. R., Kozak, M. M., Johnson, T. M., Lin, C. Y., Lin, C. J., Swiderski, D. L., Vogel, H. et al. (2014). Inappropriate p53 activation during development induces features of CHARGE syndrome. *Nature* **514**, 228-232. doi:10.1038/nature13585
- Vihhtelic, T. S., Yamamoto, Y., Sweeney, M. T., Jeffery, W. R. and Hyde, D. R. (2001). Arrested differentiation and epithelial cell degeneration in zebrafish lens mutants. *Dev. Dyn.* **222**, 625-636. doi:10.1002/dvdy.1217
- Walter, P. and Ron, D. (2011). The unfolded protein response: from stress pathway to homeostatic regulation. *Science* **334**, 1081-1086. doi:10.1126/science.1209038
- Wang, S. and Kaufman, R. J. (2012). The impact of the unfolded protein response on human disease. *J. Cell Biol.* **197**, 857-867. doi:10.1083/jcb.201110131
- Wang, B., Rong, X., Zhou, Y., Liu, Y., Sun, J., Zhao, B., Deng, B., Lu, L., Li, Y. et al. (2021). Eukaryotic initiation factor 4A3 inhibits Wnt/ β -catenin signaling and regulates axis formation in zebrafish embryos. *Development* **148**, dev198101. doi:10.1242/dev.198101
- White, R. J., Collins, J. E., Sealy, I. M., Wali, N., Dooley, C. M., Digby, Z., Stemple, D. L., Murphy, D. N., Billis, K., Hourlier, T., et al. (2017). A high-resolution mRNA expression time course of embryonic development in zebrafish. *eLife* **6**, e30860. doi:10.7554/eLife.30860
- Yamaguchi, M., Fujimori-Tonou, N., Yoshimura, Y., Kishi, T., Okamoto, H. and Masai, I. (2008). Mutation of DNA primase causes extensive apoptosis of retinal neurons through the activation of DNA damage checkpoint and tumor suppressor p53. *Development* **135**, 1247-1257. doi:10.1242/dev.011015
- Yan, Y.-L., Miller, C. T., Nissen, R. M., Singer, A., Liu, D., Kirn, A., Draper, B., Willoughby, J., Morcos, P. A., Amsterdam, A. et al. (2002). A zebrafish *sox9* gene required for cartilage morphogenesis. *Development* **129**, 5065-5079. doi:10.1242/dev.129.21.5065
- Yan, Y. L., Willoughby, J., Liu, D., Crump, J. G., Wilson, C., Miller, C. T., Singer, A., Kimmel, C., Westerfield, M. and Postlethwait, J. H. (2005). A pair of Sox: distinct and overlapping functions of zebrafish *sox9* co-orthologs in craniofacial and pectoral fin development. *Development* **132**, 1069-1083. doi:10.1242/dev.01674
- Yoshida, H., Matsui, T., Yamamoto, A., Okada, T. and Mori, K. (2001). XBP1 mRNA is induced by ATF6 and spliced by IRE1 in response to ER stress to produce a highly active transcription factor. *Cell* **107**, 881-891. doi:10.1016/S0092-8674(01)00611-0

Fig.S1

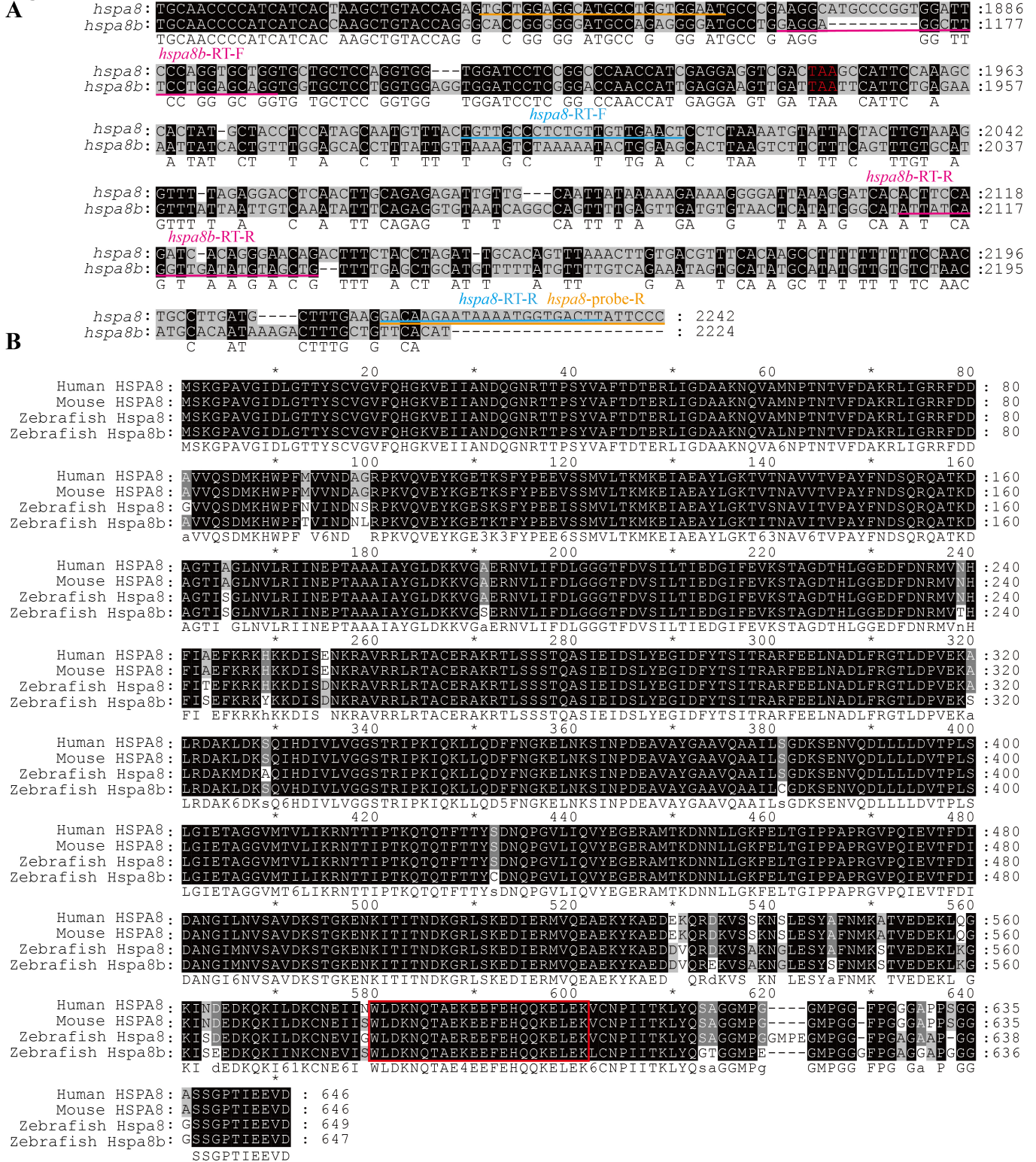
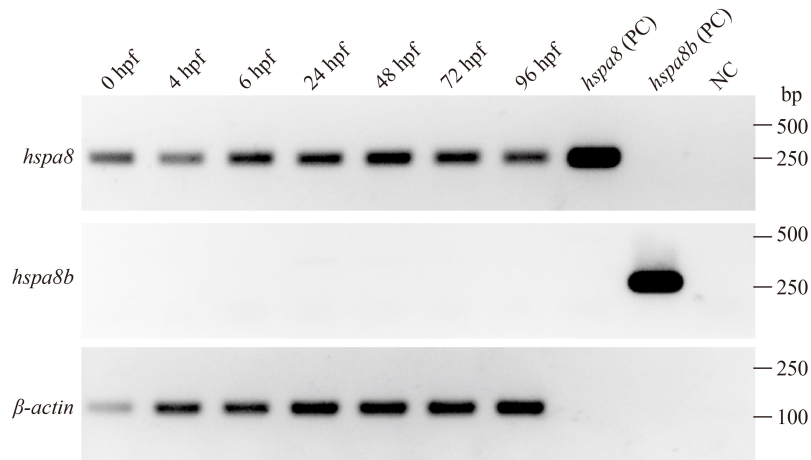


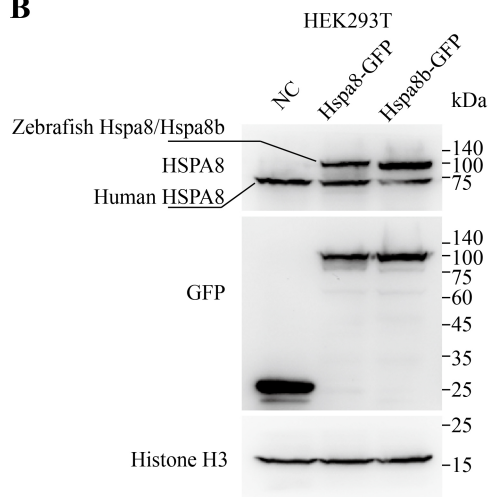
Fig. S1. Sequence alignment. (A) Comparison of the sequence of partial open-reading frame and 3' UTR region from *hspa8* and *hspa8b*. The specific primers for RT-PCR analysis and riboprobes generation were underlined. (B) Amino acid sequence alignment of human HSPA8, mouse HSPA8, and zebrafish Hspa8 and Hspa8b. The epitope that anti-HSPA8 antibody was against is highlighted with a red box. Accession numbers are: human HSPA8 NP_006588.1, mouse HSPA8 NP_112442.2, and zebrafish Hspa8 NP_001103873.1 and Hspa8b NP_001186941.1.

Fig.S2

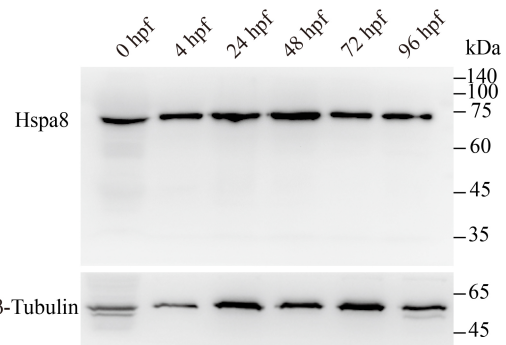
A



B



C



D

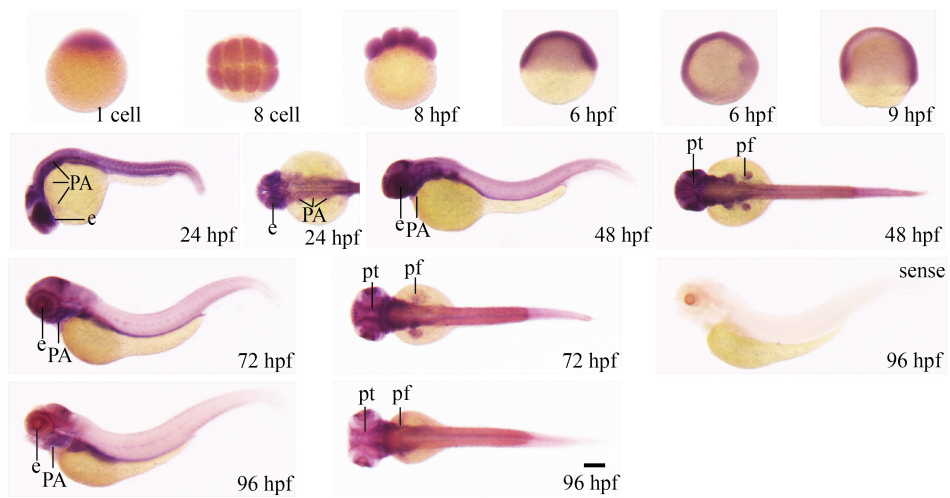


Fig. S2. Spatiotemporal expression pattern of zebrafish *hspa8*. (A) RT-PCR analysis of zebrafish *hspa8* and *hspa8b* mRNAs at the indicated embryonic stages. Numbers indicate different developmental stages as hours post fertilization (hpf). *β-actin* was used as an internal control. PC, positive control; NC, negative control. (B) Antibody validation. Plasmids encoding GFP-tagged Hspa8 or Hspa8b were transfected into HEK293T cells. After 24h, the cell extracts were subjected to western blot analysis with an anti-GFP antibody or an anti-HSPA8 antibody. (C) Hspa8 protein level in the indicated embryonic stages. Numbers indicate different developmental stages as hours post fertilization (hpf). *β-Tubulin* was used as an internal control. (D) Whole-amount *in situ* hybridization analysis of zebrafish *hspa8* mRNA at the indicated stages. Panels represent the dorsal, top, or lateral views with animal pole up or anterior to the left. e, eye; PA, pharyngeal arches; pf, pectoral fin; pt, posterior tectum. Scale bar = 200 μ m.

Fig.S3

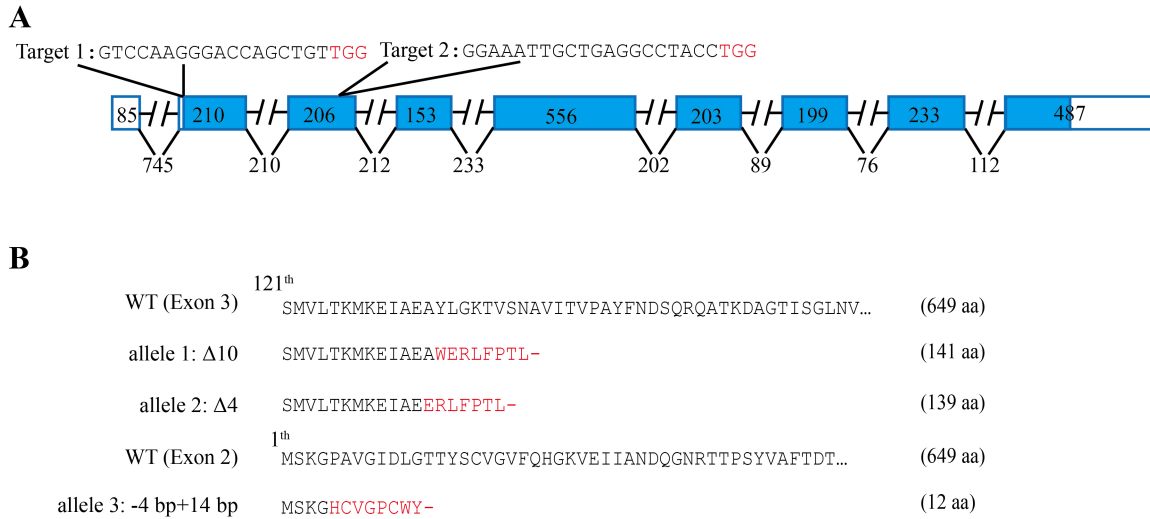


Fig. S3. Generation of *hspa8* mutants using the CRISPR/Cas9 system. (A) Schematic representation of the *hspa8* locus. Exons are shown as boxes, while introns are shown as lines. Diagram showing the CRISPR/Cas9 target DNA sequence of zebrafish *hspa8*. Protospacer adjacent motif (PAM) region is shown in red. (B) The predicted protein sequences of WT and mutant *hspa8* alleles (allele1, allele2, and allele3). The protein sequences of WT and mutants are shown.

Fig.S4

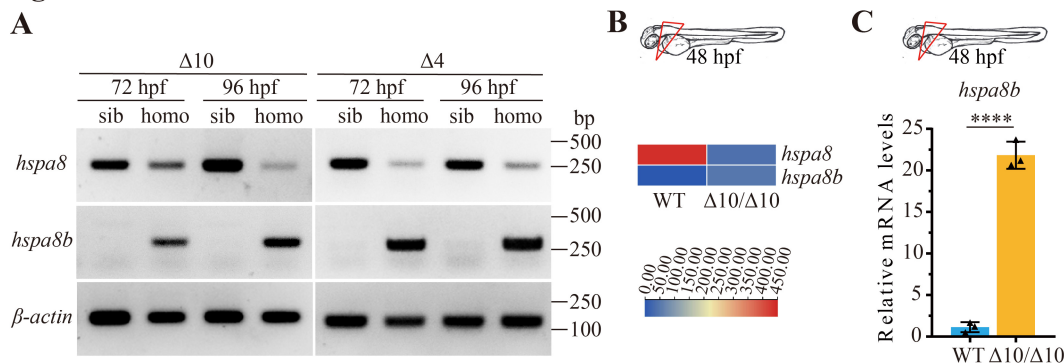


Fig. S4. Depletion of Hspa8 increases the transcription of *hspa8b*. (A) The mRNA levels of *hspa8* or *hspa8b* in siblings and *hspa8* mutants as indicated by semi-quantitative RT-PCR analysis. *β-actin* was used as an internal control. Similar results were obtained from three experiments. (B) Heatmaps of transcripts show the expression of *hspa8* and *hspa8b* in the PAs of WT sibling and *hspa8* mutant embryos at 48 hpf. (C) Relative mRNA levels of *hspa8b* in the PAs of WT sibling and *hspa8* mutant embryos at 48 hpf, as indicated by qRT-PCR analysis. Values are represented as means \pm SD. ($n = 3$). **** $p < 0.001$. Unpaired t -test, two-tailed.

Fig.S5

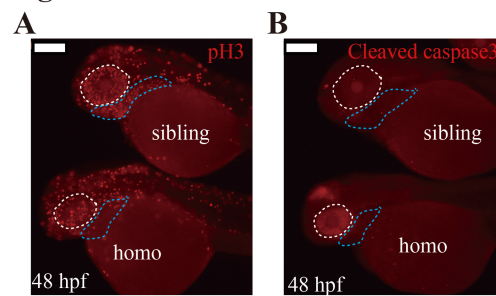


Fig. S5. Detection of cell proliferation or apoptosis in the anterior structures of zebrafish embryos. (A) Representative image of pH3-positive cells in the anterior structures of siblings and *hspa8*^{A10/A10} mutants at 48 hpf. Embryos were immunostained with an anti-pH3 antibody. (B) Representative image of apoptotic cells in the anterior structures of siblings and *hspa8*^{A10/A10} mutants at 48 hpf. Embryos were immunostained with an anti-cleaved caspase 3 antibody. The white and blue dashed lines define the eyes and pharyngeal regions, respectively. Scale bar = 200 μ m.

Fig. S6

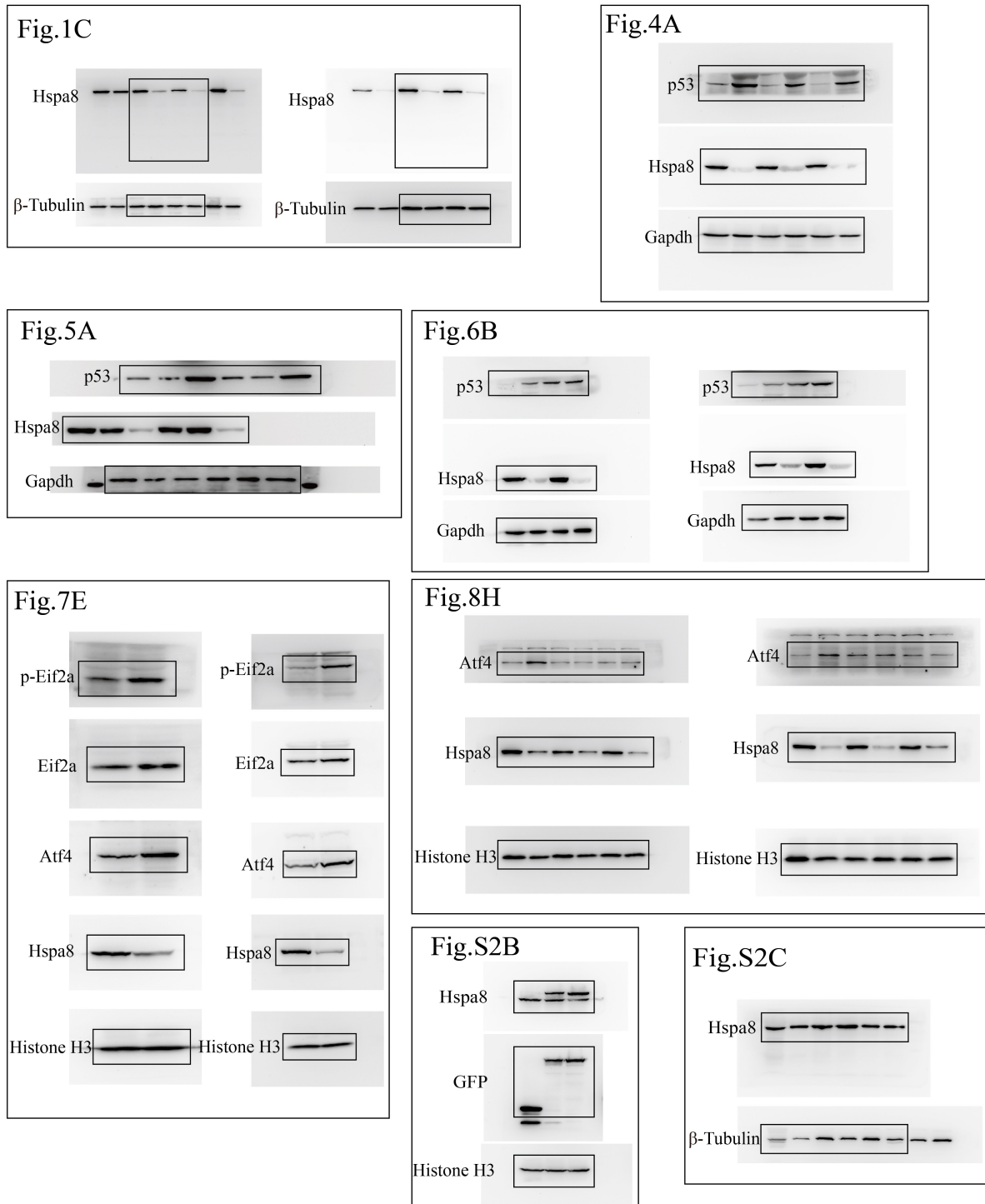


Fig. S6. Blot transparency.

Table S1. List of downregulated and upregulated genes in the pharyngeal arch region of Hspa8-depleted embryos at 48 hpf

[Click here to download Table S1](#)